Three-dimensional models of chemotherapeutic agent transport in tumours

Szabolcs Modok, MD

Ph.D. thesis

2010

Three-dimensional models of chemotherapeutic agent transport in tumours

Szabolcs Modok, MD

Ph.D. thesis

2010

Haematology Division, 2nd Department of Medicine, Albert Szent-Györgyi Clinical Centre, University of Szeged

Oxford Drug Resistance Group, Nuffield Department of Clinical Laboratory Sciences, University of Oxford

List of publications presented in the thesis

I. **Modok S**, Hyde P, Mellor HR, Roose T, Callaghan R. Diffusivity and distribution of vinblastine in three-dimensional tumour tissue: experimental and mathematical modelling. Eur J Cancer. 2006 Sep;42(14):2404-13.

II. **Modok S**, Scott R, Alderden RA, Hall MD, Mellor HR, Bohic S, Roose T, Hambley TW, Callaghan R. Transport kinetics of four- and six-coordinate platinum compounds in the multicell layer tumour model. Br J Cancer. 2007 Jul 16;97(2):194-200.

III. **Modok S**, Mellor HR, Callaghan R. Modulation of multidrug resistance efflux pump activity to overcome chemoresistance in cancer. Curr Opin Pharmacol. 2006 Aug;6(4):350-4. Epub 2006 May 11.

IV. Mellor HR, Snelling S, Hall MD, **Modok S**, Jaffar M, Hambley TW, Callaghan R. The influence of tumour microenvironmental factors on the efficacy of cisplatin and novel platinum(IV) complexes. Biochem Pharmacol. 2005 Oct 15;70(8):1137-46.

V. Alderden RA, Mellor HR, **Modok S**, Hambley TW, Callaghan R. Cytotoxic efficacy of an anthraquinone linked platinum anticancer drug. Biochem Pharmacol. 2006 Apr 14;71(8):1136-45.

VI. Alderden RA, Mellor HR, **Modok S**, Hall MD, Sutton SR, Newville MG, Callaghan R, Hambley TW. Elemental tomography of cancer-cell spheroids reveals incomplete uptake of both platinum(II) and platinum(IV) complexes. J Am Chem Soc. 2007 Nov 7;129(44):13400-1.

Presentation directly related to the thesis

VII. **Modok S**. The slow transport of vinblastine in tumour tissue models: is it a handicap or advantage? NCRI Cancer Conference, 2-5 Oct 2005, Birmingham, UK

List of abbreviations

PTFE: polytetrafluoroethylene

MCL: multicell layer

PBS: phosphate buffered saline

NSB: non-specific binding

MCR: multicellular resistance

DC: donor compartment

RC: receiver compartment

“en”: ethane-1,2-diamine

[^{14}C]-Pt(II): [^{14}C]-*cis*-[$PtCl_2$(en)]

[^{14}C]-Pt(IV): [^{14}C]-*cis*, *trans*-[$PtCl_2(OH)_2$(en)]

SRIXE: synchrotron resonance induced X-ray emission

MM: molar mass

MR: molecular radius

MTC: mass transfer coefficient

D_c: diffusion coefficient

CED: convection enhanced delivery

FRAP: Fluorescence recovery after photobleaching

ABC: ATP binding cassette

P-gp: P-glycoprotein

TS: Tumour spheroid

IV: intravenous

ROI: region of interest

Table of Content

1. Introduction

Cancer cells evade chemotherapy in many different ways and research into drug resistance mechanisms is an important driving force for anticancer drug development. Since the dawn of chemotherapy in the 1940's, many cellular resistance mechanisms have been observed, yet there are only a few agents capable of "disarming" these mechanisms.

The lack of efficacy of pharmacological multidrug resistance inhibitors in clinical studies has been attributed to numerous factors (reviewed in [1]) and has generated a certain degree of scepticism on the role of multidrug transporters. In an effort to resolve the disparity between *in vitro* evidence and clinical observations, our research team have employed a two-pronged approach, *i.e.* to further clarify the structure-function relationship of multidrug transporters (related publications [2-5]) and to examine the effect of the three dimensional multicellular architecture of tumours on multidrug transporter function, inhibition and citotoxic drug distribution. Exploration of this latter field provides the leading theme of this thesis.

Solid tumours display not only inducible unicellular mechanisms (e.g. efflux pumps) to escape cytotoxic effects but a number of inherent properties that confer resistance. The inherent, or multicellular resistance (MCR), is produced by high cell density and extensive cell-cell contact in the 3-D arrangement of cancer cells. These factors ensure slow penetration of chemotherapeutics through the solid tumour [6-7]. Despite neo-angiogenesis, the intercapillary distance in tumours remains greater than observed in normal tissues [8]. In addition, the blood flow in these new and irregularly formed vessels is often turbulent, or intermittent [9]. The inadequate vascularisation results in increased interstitial pressure due to decreased drainage of extracellular fluids (for review see [10]). The decreased filtration renders diffusion down the concentration gradient as the major driving force in achieving significant drug penetration through the avascular tumour regions.

The tumour spheroid (TS) model of avascular regions of solid tumours has been applied to investigate the distribution of drugs and novel compounds [11-12]. However, quantification of data from experiments with TS is difficult to achieve and the multicell layer (MCL) model is better suited to measure flux and to quantify transport. The MCL model comprises several layers of cancer cells grown on a semiporous membrane within a cylindrical culture well insert [13]. The system has been used to measure flux of chemotherapeutics [7, 14-15]. The

route for drug transport in MCL is mainly extracellular, and this can be hindered by several factors including cellular uptake [16-17] and metabolism of drugs [15]. However, the flux kinetics of chemotherapeutics have only been extensively analysed for tirapazamine. Therefore, vital information about the relative contributions of diffusivity, convection, cellular uptake and metabolism to intra-tumoural drug kinetics is still missing. Mathematical modelling can facilitate the dissection of penetration/flux kinetics and allow the description of processes with widely applicable parameters such as diffusion coefficient.

Fluorescence recovery after photobleaching (FRAP) is a well described *in vitro* method to measure diffusion coefficients of therapeutics in tumour tissue, however it is only suitable for macromolecules, such as antibodies, vectors etc [18-19].

1.1. Vinblastine transport studies

Vinca alkaloids are strictly cell cycle specific chemotherapeutics, as they act by slowing the dynamics of microtubule polymerisation, which is necessary for coordinated segregation of chromosomes in metaphase [20]. After IV administration vinblastine has a large volume of distribution suggesting quick absorption of the drug into the tissues. In contrast, vinblastine was the slowest of a panel of cytostatic drugs to pass through multicell layers (MCL) [7].

The multidrug efflux pump P-gp is known to limit the efficacy of vinblastine [21]. P-gp (ABC^{B1}) is an ABC transporter, whose expression has prognostic value in many cancers [22]. Inhibition of P-gp was shown to increase accumulation of P-gp substrates in deeper layers of spheroids [13] and to decrease penetration of doxorubicin through MCL [17].

However, the cell lines used in these investigations had previously been selected for high level P-gp expression. Clinical samples from drug resistant tumours are believed to display considerably lower ABC transporter expression [23]. Consequently, a long-standing debate on the precise contribution of P-gp in affecting drug distribution in solid tumours *in vivo* remains unresolved. Investigations have demonstrated that the expression of P-gp is most prevalent in the deeper layers of TS that are known to display (i) an altered microenvironment and (ii) insensitivity to chemotherapeutic drugs [24].

The aim of the present investigation was to provide detailed flux constants for vinblastine through DLD1 MCL with P-gp expression levels relevant to human tumour samples. The flux

of sucrose was determined to provide a measure of exclusively interstitial diffusion. Furthermore, the measured diffusivity of vinblastine was used to estimate its tissue distribution.

1.2. Platinum compound transport studies

Platinum drug complexes have been in clinical use for three decades and their greatest curative potential is exhibited towards certain subtypes of testicular cancer. The Pt-complexes are widely used in cancer chemotherapy but unfortunately their efficacy is limited against the majority of malignancies. The reasons for the failure of this important class of chemotherapeutic agent are a combination of cellular drug resistance, toxicity and poor whole body or cellular pharmacokinetic profiles [25]. Cellular resistance to Pt-drugs is largely attributed to up-regulation of DNA repair pathways, low intracellular accumulation and inactivation by thiol containing reductants such as glutathione and metallothionein. Toxicity of cisplatin and its four-coordinate derivatives is due to inherently high reactivity, which leads to premature adduct formation with nucleophilic groups on macromolecules [26]. The reactivity results from "aquation" caused by the exchange of Cl^- moieties for OH^- in a low chloride environment, such as that in the intracellular milieu. The activation will ultimately manifest as the side effect profile in addition to ensuring that only a minor fraction of the plasma platinum dose will be available to form adducts with the DNA [27]. Platinum exists in a number of ionisation states and the presence of axial ligands in the six coordinate Pt(IV) complexes has generated a series of compounds with considerably lower "aquation" rates [28]. The resultant increased stability and reduced covalent binding to serum proteins [28], facilitates delivery of Pt(IV) drug to cancer cells at effective concentrations.

The efficacy of Pt(II)-complexes is severely limited due to poor cellular uptake. The main pathway for intracellular accumulation of Pt-drugs is thought to be passive diffusion through the plasma membrane [29], although the Ctr1 copper importer [30] and the copper export pump ATP7B [31] have also been implicated. The introduction of hydrophobic axial ligands in Pt(IV)-complexes was thought to provide a strategy to facilitate passive diffusion into cancer cells. Unfortunately, the correlation between lipophilicity and cellular uptake was weak for Pt(IV) compounds [32], though amongst a range of Pt(IV) compounds *cis,trans*-$[PtCl_2(OH)_2(en)]$ was the least lipophilic (log P_{oct} : -2.78) and had the lowest cellular uptake. In contrast, there was a better correlation between the redox potential and uptake of these compounds. This finding has generated a model, which proposes that the Pt(IV) drug exists in

a dynamic equilibrium across the cell membrane and that the preferable rate of intracellular "aquation" and subsequent reactivity effectively traps the drug inside the cell [32].

Yet despite the many advantageous features of Pt(IV)-complexes that have been demonstrated in monolayer cultures of cancer cells, there are few of this class of drug in clinical use. A possible explanation for this lack of translation may be the complexity of solid tumours *in vivo*, relative to the *in vitro* experimental system. Tumours *in vivo* represent complex 3-D cellular organisations with a characteristically harsh microenvironment comprising high cell density, low pH, toxic metabolites, low oxygenation and elevated interstitial pressure. Few studies have systematically examined the impact of these and other factors on the efficacy of Pt(IV)-complexes in solid tumours or provided information on the distribution, diffusivity and flux of Pt(IV)-complexes through a solid tumour. It is known that the driving force for passive diffusion through the plasma membrane is the concentration gradient of the platinum compound. Hence increased penetration of Pt(IV)-complexes into tumour tissues, a higher local drug concentration and rapid intracellular aquation may significantly impact on the delivery of platinum compounds to nuclear DNA.

The present investigation has examined the pharmacokinetic properties of a reductively activated Pt(IV) compound in the multicellular layer three-dimensional tumour model. This model enabled a quantitative analysis of the distribution and flux parameters for Pt-drugs [33]. The data verified a mathematical model developed to describe drug pharmacokinetics within solid tissue. Moreover, a novel elemental imaging analysis by synchrotron radiation induced X-ray emission was applied to examine Pt-distribution and the degree of intacellular accumulation in multicell layers.

2. Aims

I. To set up a 3-D tumour model suitable for measuring drug diffusivity in tissue.

II. To characterise this experimental system, *i.e.* the MCLs in terms of morphology, cell proliferation and tissue hypoxia, ABC transporter expression at protein and mRNA level.

III. To utilise the MCLs and optimise conditions to make it a versatile assay of drug transport and distribution.

IV. Simultaneuosly mathematical modelling was pursued to facilitate quantification of results from drug transport experiments. Initially we aimed to describe the inherent characteristics of the transport system with and without the MCL.

V. Mathematical modelling was necessary to quantify drug diffusivity, distribution and cellular uptake in the MCL.

VI. Utilising the experimental and mathemathical model we aimed to describe the transport of a typical ABC transporter substrate *e.g.* vinblastine.

VII. We aimed to describe the transport of a novel six-coodinate platinum compound and compare it to that of a four-coordinate compound, which is similar to cisplatin.

VIII. The possibility to increase platinum drug penetration by increasing hydrostatic pressure was investigated.

IX. We aimed to experimentally determine drug distribution profile within the MCL and compare it to predictions of the mathematical model.

X. Finally, we aimed to mathematically model cytotoxic drug penetration and distribution in a simplified *in silico* 3-D tumour model.

3. Materials and Methods

3.1. Materials

[^{3}H]-vinblastine sulphate (10.8 Ci/mmol) and [U-^{14}C]-sucrose (601-660 Ci/mol) were purchased from Amersham Biosciences (Little Chalfont, UK). [^{3}H]-vinblastine was prepared in methanol and the final solvent concentration was kept below 1% in each experiment. [^{14}C]-[$PtCl_2$(en)] (34 Ci/mol) (Figure 1a) and [^{14}C]-*cis,trans*-[$PtCl_2(OH)_2$(en)] (6.8 Ci/mol) (Figure 1b) were synthesised according to published methods [34].

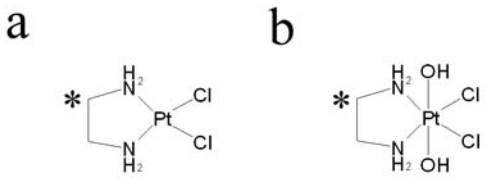

Figure 1 The chemical structures of the four (c; [^{14}C]-cis-[$PtCl_2$(en)]) and six-coordinate platinum compounds (b; [^{14}C]-cis,trans-[$PtCl_2(OH)_2$(en)]). * indicates the position of the ^{14}Carbon radio isotopes.

Platinum compounds were dissolved in 100 mM KCl in ddH_2O at 0.5 mM concentration and stored in aliquots at -20°C. 24-well culture plates and Transwell-Col inserts (polystyrene sidewall, 6.5 mm internal diameter, bovine placental collagen type I and III coated polytetrafluoroethylene (PTFE) membrane, 0.33 cm^2 surface, 400 nm average pore size) were from Corning Life Sciences (Schiphol-Rijk, The Netherlands). Penicillin and streptomycin were from Cambrex Bioscience (Verviers, France), spinner flasks were from Techne Ltd (Cambridge, UK). All other cell culture materials were from Invitrogen (Paisley, UK). OCT, haematoxylin and eosin were from RA Lamb (Eastbourne, UK). Agarose was purchased from BioWhittaker Biological Applications (Rockland, ME), and Ready Protein + scintillation fluid was from Beckman Coulter Inc. (Fullerton, CA). Benzamidine, leupeptin and pepstatin were from Calbiochem (Merck Biosciences, Nottingham, UK). ECL Western Blotting Detection Kit was from Amersham Biosciences (Little Chalfont, UK). The C219 anti-human P-gp antibody was purchased from CIS (Gif-Sur-Yvette, France), MIB1 anti-Ki67 antibody and

Aquamount were obtained from DAKOCytomation (Ely, UK), MACH2 horse-radish peroxidase labelled anti-mouse secondary antibody was bought from Biocare Medical (Concord, USA) and DAKO Peroxidase blocking reagent was from DAKO Corporation (Carpintier, USA). Hypoxyprobe™-1 kit was purchased from Chemicon Europe Ltd, UK, Brij 35 from Fisher Scientific, UK. RLT buffer and DNase were from Qiagen (Crawley, UK). Biorad DC protein assay kit was purchased from Biorad (Hercules, USA). All other chemicals were at least analytical grade and were purchased from Sigma.

3.2. Cell lines and MCL culture

Caco2, $MCF7^{WT}$, NCI/ADR^{Res} and DLD1 cells were cultured as monolayers according to ATCC and previously published protocols [21, 34]. To generate MCL, DLD1 cell monolayers were detached from culture flasks with trypsin/EDTA and 3 x 10^5 cells were seeded into Transwell-Col inserts. After a few hours the cells had settled and the inserts were transferred into spinner flasks with 50 mL RPMI 1640 medium per insert. Half of the medium was refreshed every third day until the MCL were harvested.

3.3. Morphological characterisation of MCL

MCL were fixed in 4% buffered paraformaldehyde and 4 % agarose was layered on both sides to prevent folding of the MCL during subsequent processing. To facilitate the orientation during wax embedding, MCL were cut out from the insert and cast into square agarose blocks in the base of a square plastic cuvette. MCL were dehydrated through routine histological processing, embedded in paraffin wax and 5 μm sections were cut. Sections were allowed to dry overnight and stained with haematoxylin and eosin to assess general morphology. The thickness of MCL and the PTFE membrane on cross sections was measured with a calibrated eyepiece graticule [34].

3.4. Detection of proliferating cells by Ki-67 immunohistochemistry

Paraffin sections of MCL were dewaxed and after antigen retrieval (30 s at 120°C in 10 mM Tris, 1 mM Na_2EDTA, pH 9.0 buffer) stained for Ki-67 [35]. Briefly, the slides were incubated for 15 min at room temperature with DAKO Peroxidase blocking reagent in a humidified chamber. To reduce non-specific binding, slides were incubated for 30 min in PBST with 1 % BSA. The sections were incubated for 1 hour with the MIB1 mouse antibody in PBST with 1 % BSA, then for 1 hour with an HRP labelled anti-mouse secondary antibody

(MACH 2). Signal was then developed with 3,3'-diaminobenzidine chromogen. Nuclei were counterstained with heamatoxylin and sections were mounted in Aquamount.

3.5. Detection of hypoxia in MCL

MCL were incubated with 200 μM pimonidazole (Hypoxyprobe-1) in culture medium for 2 hours and then fixed in 4% buffered paraformaldehyde. The fixed MCLs were extracted and embedded in 4% agarose as described in chapter 3.3. MCLs in agarose moulds were dehydrated through routine histological processing and embedded in paraffin for subsequent sectioning (5 μm). Sections were de-waxed, rehydrated with PBS, washed with PBS/0.2% Brij 35 and antigen retrieval achieved with 0.01% Pronase at 40ºC for 40 min. Sections were washed with PBS/0.2% Brij 35 at 4ºC between all subsequent steps. Endogenous proxidase activity was inhibited with Peroxidazed 1 (BioCarta, Europe) and the primary antibody (Hypoxyprobe-1 Mab1) was added for 40 min at 25ºC. Mach 2 goat-anti-mouse HRP conjugate (BioCarta, Europe) was added for 45 min and detection was achieved using DAB substrate chromogen (DakoCytomation, UK). Sections were counterstained with haematoxylin and mounted with aquamount.

3.6. Detection of mdr1 mRNA expression by real-time quantitative TaqMan RT-PCR

Trypsinised DLD1, Caco2, $MCF7^{WT}$ and NCI/ADR^{Res} cells from monolayer cultures were resuspended in RLT buffer containing 1% β-mercaptoethanol and total mRNA extracted according to RNeasy Mini protocol from Qiagen. The residual DNA was digested on the column with DNase. Levels of *mdr1* mRNA were quantified by real-time quantitative TaqMan RT-PCR using the ABI Prism 7700 Sequence Detection System, Sequence Detector v1.6.3 software (Applied Biosystems, Warrington, Cheshire, UK). The following oligonucleotides were designed with Primer Express Software version 1.0 (Applied Biosystems) and were a kind gift of Dr. Steve Hyde (NDCLS, University of Oxford): forward *mdr1* primer, TGG TTC AGG TGG CTC TG; reverse *mdr1* primer, CTG TAG ACA AAC GAT GAG CTA TCA CA; FAM labelled *mdr1* probe, AGG CCA GAA AAG GTC GGA CCA CCA. 18S rRNA was quantified as the endogenous control using the following oligonucleotides: forward rRNA primer, CGG CTA CCA CAT CCA AG GAA; reverse rRNA primer, GCT GGA ATT ACC GCG GCT; VIC labelled rRNA probe, TGC TGG CAC CAG ACT TGC CCT C. To match expected expression levels, 100 ng total RNA for *mdr1* mRNA and 5 ng for rRNA was reverse transcribed. Subsequently, each sample was subjected

to TaqMan PCR according to previously published protocols [36]. Relative expression levels were calculated using the $\Delta\Delta C_T$ method.

3.7. Detection of P-gp protein expression in DLD1 monolayer cultures and MCL by western blotting

Both monolayer and MCL cultures of DLD1 cells were briefly trypsinised and lysed in phosphate buffered saline (PBS) with 2 % SDS and protease inhibitors (1 mM benzamidine, 20 μM leupeptin and 1 μM pepstatin). Total protein concentration was determined using the Biorad DC protein assay kit and P-gp expression was detected by western blotting as previously described [37] using purified P-gp from CHO^{B30} cells as a positive control.

3.8. Determination of flux of radiolabelled compounds through MCL

Inserts with MCL were transferred into 24-well plates with 1 mL fresh medium in the wells (Fig. 2). When the insert was moved to a new well, the medium in the donor compartment (DC) was replaced by 150 μL of fresh RPMI 1640 medium containing [^{14}C]-sucrose and [^{3}H]-vinblastine-sulphate or a [^{14}C]-labelled platinum compound. During transport studies with platinum compounds the RC was not stirred since the flux rates across the membrane were identical with or without stirring (data not shown). An agarose overlay has previously been used in RC to eliminate convection in a floating insert [7, 16-17]. Unfortunately the presence of agarose in the RC has been reported to slow down diffusion [15]. The present experimental set-up was able to eliminate convective terms since the insert was kept stable in the culture well and fluid levels in the two compartments were equal thus resulting in zero fluid pressure gradients (and therefore no convection) across the MCL. In certain experiments, to provide convective force against the concentration gradient driven diffusion, the volume of the RC was increased to 1500 μL. The reverse gradient was created by increasing the DC volume to 280 μL and keeping the RC at 1000 μL. These two configurations provide ± 3 mm H_2O hydrostatic pressure between the two compartments. The entire experimental apparatus was placed into an incubator to maintain standard MCL culture conditions. These conditions were used throughout the investigations to minimise temperature gradient driven convection.

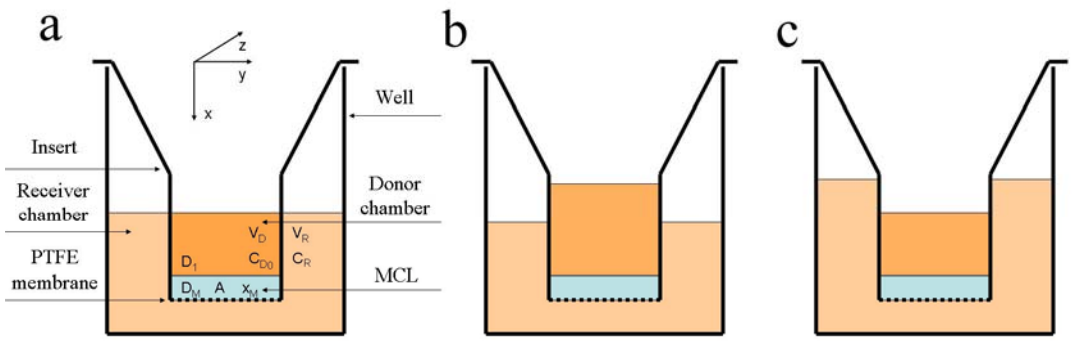

Figure 2 The experimental set-up for the drug transport assay is illustrated on a cross section of a well on a 24-well plate with the insert (a). The donor and receiver chambers are separated by the polystyrene wall of the cylindrical insert and the membrane with or without the MCL. The letters and indices correspond to variables used in the mathematical modelling (see Appendix). Unless it is otherwise specified in all experiments the fluid levels in donor and receiver chambers were equal (a). However, in certain experiments the culture medium containing the radiolabelled compounds was added to the donor compartment in variable fluid volumes (b and c). Fluxes were measured by taking samples form the receiver compartment.

At specific times during the assay, the insert was moved to a new well with fresh culture medium, which could potentially induce some convective disturbance [38]. However, the timescale of these events is very short compared to the length of the transport assay therefore they are unlikely to influence our measurements. To measure diffusive flux of the compounds from the DC through the MCL, 800 μL samples were taken from each of the used wells. The amount of radiolabelled compound was determined by liquid scintillation counting after the addition of 4 mL Ready Protein+ scintillation liquid.

3.9. Non-specific binding of radiolabelled compounds to the plastic of the transport apparatus

Binding to polystyrene can confound flux values. The interaction between polystyrene and radiolabelled compounds can be defined as non-specific binding (NSB), *i.e.* non-saturable and linear with respect to drug/ligand concentration (page 238 of [39]). Consequently, the proportions of bound and free drug could be estimated at a single drug concentration for the present experimental set-up. The NSB of compounds to the lower chamber was measured by

incubating the plastic inserts in wells of a 24-well culture plate in medium containing a 9:1 ratio of cold and radiolabelled compounds. Two hours later, samples were taken from the RC to measure the amount of drug that remained in the culture medium. The amount of drug was determined by liquid scintillation counting. A similar correction was made for platinum drugs in the DC. Following completion of transport assays samples were taken from the DC and the PTFE membranes with the MCL were excised to measure bound radioactivity. In control experiments without MCLs the PFTE membrane was excised. The percent of added [^{14}C]-Pt-complex bound to the DC was determined by subtracting the percent bound to PTFE membrane in the presence or absence of the MCL, the percent transported to the RC and from the percent decrease in the DC at the end of the transport assay.

3.10. Measuring the mass transfer coefficient and relative porosity of the collagen coated PTFE membrane for [^{14}C]-sucrose, [^{3}H]-vinblastine and [^{14}C]-Platinum compounds

The PTFE membrane may itself impede flux of radiolabelled compounds through the MCL system. Consequently, the transport of radiolabelled compounds through the membrane was measured using the same experimental setup shown in Figure 2 but in the absence of the MCL. The amount of compound transported was determined by scintillation counting after 5, 10, 15, 20, 25 and 30 minutes incubation using the same set of inserts and adding fresh stock solution of the drug-containing medium. During data analysis the membrane was assumed to be semiporous with negligible thickness.

3.11. SRIXE of MCL cross sections

MCLs were harvested at the end of the transport experiment using the Pt(IV) compound, processed as described in chapter 3.3. and 20 μm sections were cut from the paraffin blocks. The sections were mounted on Formvar coated plastic specimen holders. Micro-SRIXE experiments were performed on beamline ID22 at the European Synchrotron Radiation Facility (ESRF), Grenoble, France. Fluorescence spectra were collected using a single element Si(Li) detector, placed approximately 20 mm from the sample. Two dimensional maps corresponding to the integrated Kα fluorescence signal of an element of interest were collected by scanning the sample. The elements analysed were P, S, Cl, K, Ca, Fe, Ni, Cu, Zn. Pt was analysed using the Lα and Lβ fluorescence lines. Elemental contents were quantified by comparison to the SRM 1832 and 1833 thin polymer film standards (NBS/NIST, Gaithersburg, MD, USA) using the assumption for a thin film target. Sectioned MCLs were analysed using a 13 keV monochromatic X-ray beam focused to a 1.8 μm x 4.5 μm (vertical x

horizontal) spot. Samples were mounted and suitable areas of the MCL located by viewing the sample with a video-zoom microscope. Scan areas were chosen so as to incorporate a representative cross section of the MCL. PyMca, an ESRF code, was used for fitting the acquired spectra (http://www.esrf.fr/computing/bliss/downloads/pymca/PyMCA.pdf). This allowed the background contribution to be removed, facilitated analysis of overlapping peaks, and accounted for the eventual escape peaks. X-ray lines were fitted using the Hypermet function and a model for background fitting was chosen as a 10^{th} order polynomial for an exponential background model. Computed X-ray line intensities were normalized to the value of the incident photon flux.

Data analysis of SRIXE imaging was performed by choosing regions of interest (ROIs) within each scan. Such ROIs typically included one ROI encompassing the majority of the scan area ("whole MCL"), another encompassing the free surface of the tissue (*i.e.* DC surface), and another encompassing part of the PTFE membrane (*i.e.* RC surface). The average fluorescence spectra from each ROI were fitted using the PyMca X-ray fluorescence fitting program. Elemental concentrations (μg cm^{-2}) were calculated from peak areas using peak area:concentration ratios determined from NIST thin-film standards (SRM 1832 and 1833), and then converted to μg cm^{-3} by accounting for the known section thicknesses. Such calculations neglected secondary fluorescence processes and assumed that the standards and the sample were similar to one another. The Pt-Lα fluorescence line was used to quantify platinum content in a similar fashion to that outlined by Ilinski *et al*, [40] using fluorescence line cross sections (at 13 keV) of Zn-Kα = 43.089 cm^2g^{-1}, and Pt-Lα = 18.208 cm^2g^{-1} [41]. Elemental content of ROIs were compared to that of the "whole MCL" ROI, and the zinc content of the ROI.

3.12. Data analysis

Data presented are mean ± SD or mean ± SEM. Data were analysed with ANOVA or two-tailed Student's t-test using GraphPad Prism 3.2 software and $p < 0.05$ was considered statistically significant. Diffusivity and the rate of cellular uptake were determined using programs written in Matlab 7.0.1 software based on the mathematical models described in the *Appendix*.

4. Results

4.1. Characterisation of MCL

4.1.1. Growth and Histology of MCL

The MCL system is used only in a few laboratories around the globe, furthermore it has not been used in our laboratory. Thus, we characterised it to great detail before embarking on transport experiments.

DLD1 colon adenocarcinoma cells were grown in polystyrene inserts on bovine collagen type I and II coated porous PTFE membranes that allow movement of small molecules, but prevent cells from traversing the membrane. The thickness of the PTFE membranes was measured on cross sections using an eyepiece graticule on an upright light microscope and it was 38 ± 1 µm. A minimum of 3 x 10^5 DLD1 cells were required to fully cover the PTFE membrane as a confluent monolayer.

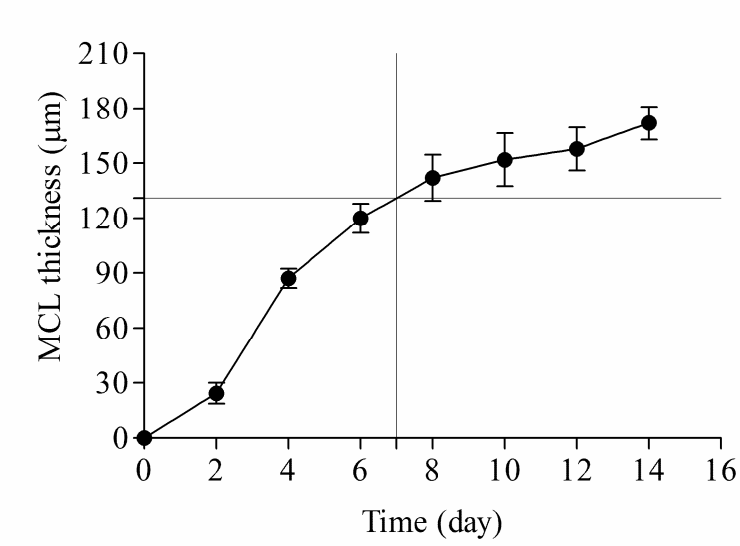

Figure 3 Growth of multicell layers was determined by seeding 3 x 10^5 DLD1 cells into several inserts and subsequent culture in spinner flasks. On specific days, MCL were harvested and processed as described in *Materials and Methods*. The thickness of haematoxylin & eosin stained cross sections was measured by a calibrated eyepiece graticule of a light microscope. The data points are mean ± SD of several measurements along several cross sections of at least 2 MCL.

As shown in Figure 3 the MCL grew exponentially from 24.3 ± 5.7 μm on day 2 and eventually the growth rate slowed down and the MCL reached a thickness of 172 ± 9 μm by the 14th day of culture. MCLs harvested on the 7th day (131± 10 μm thickness) were used in subsequent transport experiments.

The MCL generated by DLD1 cells displayed much of the cellular heterogeneity found in solid tumours (Fig. 4a). The cells close to the PTFE membrane had large cigar shaped nuclei, while those towards the "upper" surface gradually became flattened. The distribution of proliferating cells also displayed temporal and spatial heterogeneity in MCL. At early stages of MCL growth, the proliferating cells were found throughout the tissue (data not shown). At later stages of the growth curve, the non-proliferating cell mass (quiescent cell, Q) appeared in the central region of the MCL (Fig. 4b).

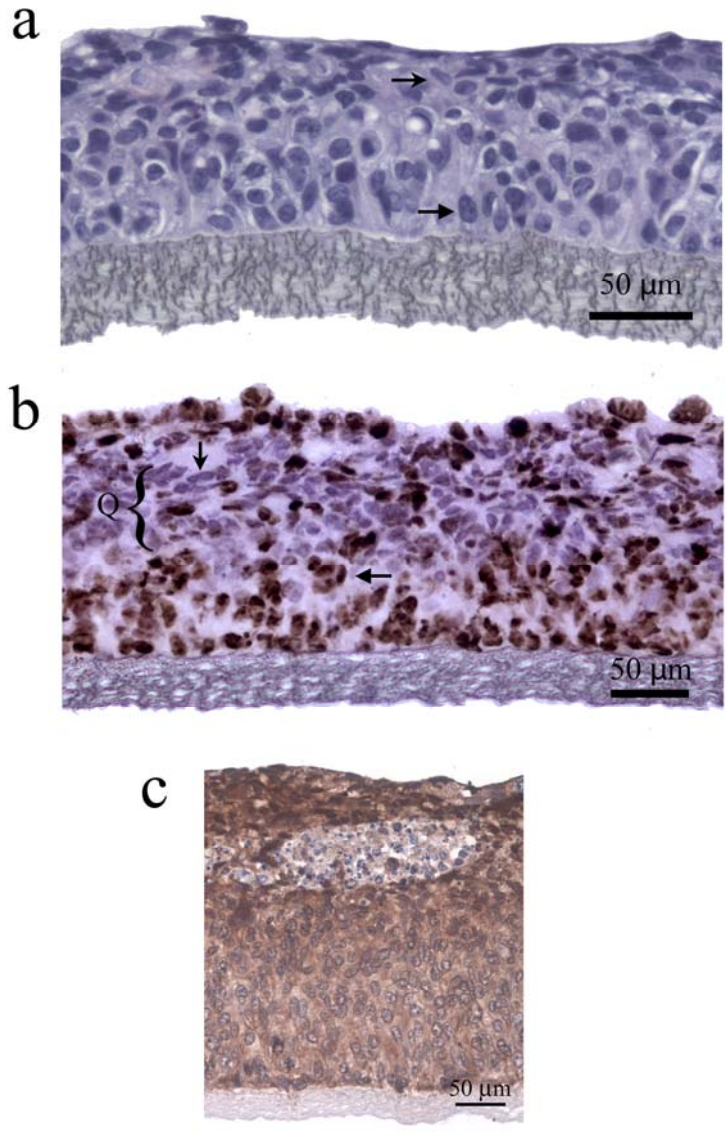

Figure 4 Cellular morphology and proliferation in DLD1 multicell layers was studied on 5 μm paraffin sections, which were either stained with H&E (a) or Ki-67 expression detected by immunohistochemistry (b). Arrows indicate cells with different nuclear morphology (a) and Ki-67 staining (b). Q indicates the quiescent area of the MCL. (c) Tissue hypoxia was detected in 16-day-old DLD1 MCLs with the hypoxia probe pimonidazole on a 5 μm paraffin cross section (all images were taken using an 40x objective) (for details see *Materials and Methods*).

A pimonidazole based assay was used to detect hypoxia in the MCL (Figure 4c). The MCL showed pimonidazole staining towards the upper surface of the tissue, which is indicative of hypoxia. This localised hypoxia may be explained by the high demand for oxygen, which results from such a densely packed avascular population of cells, similarly to that seen in tumour spheroids (see publication # IV.). This suggests that the MCL model is a good representation of solid tumour architecture and the associated microenvironment.

4.1.2. mdr1 mRNA and P-GP expression in MCL

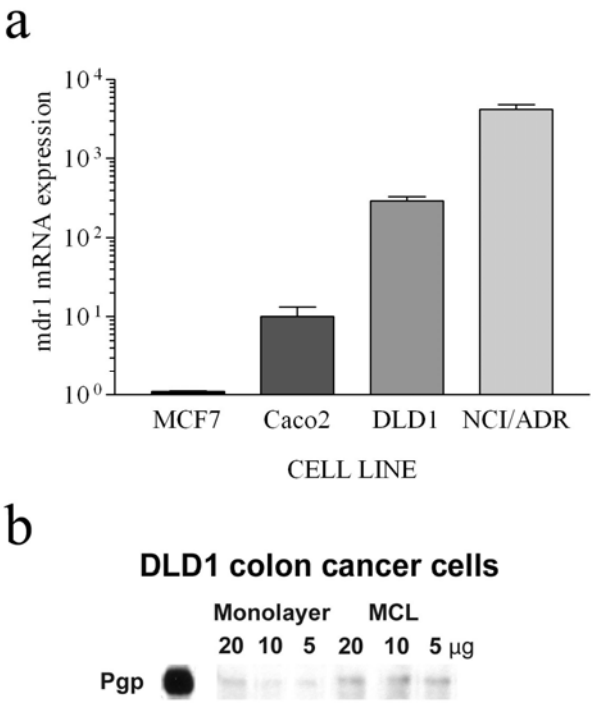

Figure 5 Relative *mdr1* mRNA and P-glycoprotein expression was studied in DLD1 cells. (a) Single cell suspension of cells were subjected to mRNA extraction and real time quantitative RT-PCR as detailed in *Materials and Methods*. Columns indicate mean ± SEM relative *mdr1* mRNA expression levels of 3 independent experiments normalised for loading differences by rRNA levels (endogenous control). (b) P-gp expression was detected by western blotting with C219 antibody on cell lysates from DLD1 monolayers and MCL. Purified hamster P-gp (2 µg) was used as a positive control.

It is well established that P-GP is expressed by normal colon epithelial cells and this expression is retained after malignant transformation [42]. P-GP can restrict the cellular

uptake of anticancer drugs, such as vinblastine in the TS model [12]. Consequently, it was necessary to characterise expression levels of P-GP in MCL grown from colon carcinoma cells. The *mdr1* mRNA levels of DLD1 cells were compared to cells known to express low ($MCF7^{WT}$), intermediate (Caco2) and high (NCI/ADR^{Res}) levels of P-gp. As shown in Figure 5a, DLD1 cells expressed levels of *mdr1* mRNA intermediate between the Caco2 and NCI/ADR^{Res} cell lines. This mRNA expression was manifest as measurable expression of the protein product (P-gp) in DLD1 cells cultured as monolayers and as MCL (Fig. 5b). Purified hamster P-gp was used as a positive control. Moreover, the relative level of P-gp expression was marginally higher when the cells were grown as MCL.

4.1.3. Correlation between MCL thickness and [^{14}C]-sucrose flux

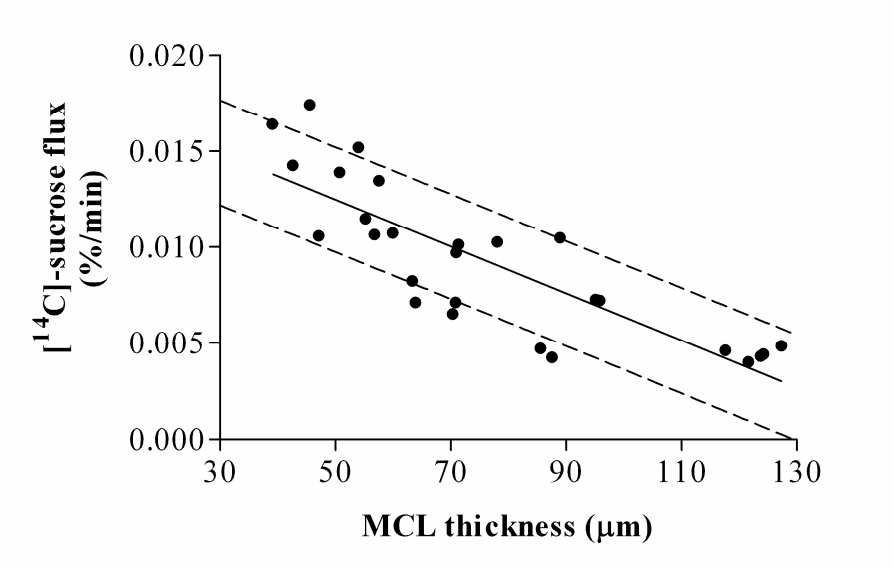

Figure 6 Correlation between the [^{14}C]-sucrose flux and the thickness of the MCL. The cumulative appearance of [^{14}C]-sucrose devided by the total amount added was plotted against time. The slope of the steady state (linear) phase was determined by linear regression and was plotted as [^{14}C]-sucrose flux (% / min) against the thickness of the MCL, which was measured as described in *Materials and Methods*. The solid and dashed lines are the linear regression and the 95% confidence intervals of the data points respectively.

The flux of [^{14}C]-sucrose through the PTFE membrane only was faster than in the presence of MCL (Fig. 7a & b, note the different scale of the y axis) and in general the [^{14}C]-sucrose flux was slower through thicker MCL (Fig. 6). However, the correlation between [^{14}C]-sucrose flux and the thickness of the MCL was weak and the age of the culture predicted the thickness of the MCL more accurately (Fig. 3). Thus MCLs were used on the 7th day of culture and

displayed a tissue depth of 131 ± 10 μm. The integrity of MCLs was checked with phase contrast microscopy before each transport experiment.

4.2. Drug transport assays

4.2.1. Mass transfer coefficient and relative porosity of the membrane

The DC and RC were separated by the polystyrene sidewall of the insert and by the collagen coated PTFE membrane in the absence of MCL in the two-compartment system (Fig. 2a). The fluids were levelled in the two compartments when 150 μL and 1000 μL media were loaded in the DC and RC respectively (Fig. 2a). The flux of radiolabelled compounds between the two compartments is hindered not only by MCL but by the PTFE membrane too. In order to quantify the membrane's relative porosity, the diffusivity of the radiolabelled compounds in the bathing medium must be ascertained. The diffusivity of sucrose in aqueous solution at 25°C has previously been measured ($5.228*10^{-6}$ cm^2s^{-1}, [43]) and this value was extrapolated to 37°C using the Stokes-Einstein equation (7.0×10^{-6} cm^2s^{-1}) [44]

$$D_1 = \frac{k_B T}{6\pi\eta R}, \qquad \text{(Equation 1)}$$

where D_1 is the diffusion coefficient, k_B is the Boltzman's constant ($1.38*10^{-23}$), T is the absolute temperature in Kelvin, η is the viscosity of water at 37°C ($6.92*10^{-8}$ Nsm^{-1}), R is the hydrodynamic radius of the molecule. The diffusivity of vinblastine (3.28×10^{-6} cm^2s^{-1}) was estimated from its molecular radius using the Stokes-Einstein equation (Equation 1) as detailed in Table 1.

The non-specific binding (NSB) of compounds to the experimental apparatus, is an acknowledged and yet often ignored problem in transport systems [16]. Consequently, the NSB of [^{14}C]-sucrose and [^{3}H]-vinblastine to the polystyrene wall of the RC was determined at concentrations used in the transport assay. After two hours 10.9 ± 1.3 % (n = 3) and 31.2 ± 1.7 % (n =3) of the administered [^{14}C]-sucrose and [^{3}H]-vinblastine were bound, respectively. The measured amount of the radiolabelled compound in the RC was corrected with the NSB for all estimations of drug flux through the MCL.

Table 1 Physical, chemical and transport parameters of radiolabelled sucrose, vinblastine and platinum compounds (results are mean ± SD)

	[^{14}C]-sucrose	[^{3}H]-vinblastine	[^{14}C]-Pt(II)	[^{14}C]-Pt(IV)
MM (g/mol)	342	811	325	359
MR (nm) [1]	0.5	1.0	0.4	0.4
D_c in medium (D_1,*10^{-6} cm^2s^{-1}) [2]	7.0	3.3	8.2	8.2
MTC (k, *10^{-5} cm s^{-1})	14 ± 3 n = 3	12 ± 3 n = 3	2.7 ± 0.6*§ n = 3	2.5 ± 0.4*§ n = 3
Relative porosity of membrane (ψ; *10^{-2})[3]	8 ± 2 n = 3	14 ± 4* n = 3	1.2 ± 0.3*§ n = 3	1.2 ± 0.2*§ n = 3
Impedance of MCL (Γ; *10^{-2}) [4]	0.60 ± 0.13 n = 3	0.57 ± 0.06 n = 3	2.1 ± 0.3*§ n = 3	2.2 ± 0.4*§ n = 4
D_c in MCL (D_M; *10^{-8} cm^2s^{-1}) [5]	4.2 ± 0.9 n = 3	1.9 ± 0.2 n = 3	17.5 ± 2.6*§ n = 3	17.8 ± 3.1*§ n = 4
Uptake rate in MCL (g; *10^{-2} min^{-1})	ND	ND	17.7 ± 5.5 n = 3	16.2 ± 5.3 n = 4

[1]The MR of sucrose was taken from a paper by Venturoli *et al* [45], MR of vinblastine was estimated based on its crystal structure [46] and on its conformation in solution [47]. The MR of Pt(II) and Pt(IV) was estimated based on the size of carboplatin (8x4x3 Å) and cisplatin (5x3x1.5 Å) as measured in MDLChime (http://www.umass.edu/microbio/chime/getchime.htm).

[2] The sources of D_c's are detailed in the relevant chapters of the thesis.

[3]The relative porosity of the membrane was calculated using Eq. 5.

[4]The impedance (Γ) was the fitted parameter in transport assays with MCL.

[5]The D_M was calculated using the equation Eq. 7.

* Values for k, ψ, Γ, D_M and g were tested with ANOVA. Using Tukey's post hoc test * indicates significant difference from sucrose, § indicates significant difference from vinblastine.

The appearance of the two labelled compounds in the RC was measured (C_R) over a 30 min period (Figure 7a). Applying the mathematical model described in the *Appendix* generated values of 14 ± 0.3 x 10^{-5} cm s^{-1} as the mass transfer coefficient for sucrose and 12 ± 0.3 x 10^{-5} cm s^{-1} for vinblastine (Table 1). The relative porosity of the collagen coated PTFE membrane

was calculated using Equation 5 (*Appendix*) and it was almost two fold higher for [^{3}H]-vinblastine ($14 \pm 4 \times 10^{-2}$), than for [^{14}C]-sucrose ($8 \pm 2 \times 10^{-2}$) ($p < 0.05$) (Table 1).

4.2.2. Diffusive transport of [^{14}C]-sucrose and [^{3}H]-vinblastine in the MCL

Information on the relative porosity of the PTFE membrane enabled the accurate characterisation of the diffusivity of the compounds in the MCL. Flux of sucrose through the MCL is exclusively through extracellular diffusion, since (i) disaccharides cannot be taken up directly by the cells and (ii) colon cancer cells do not express the brush border enzyme sucrase-isomaltase that is responsible for its digestion in intestinal mucosa [48]. [^{14}C]-sucrose flux was used as an indicator of interstitial diffusion and its diffusion coefficient in the MCL interstitium was calculated to be $4.2 \pm 0.9 \times 10^{-8}$ cm^2 s^{-1} using the mathematical model described in *Appendix*.

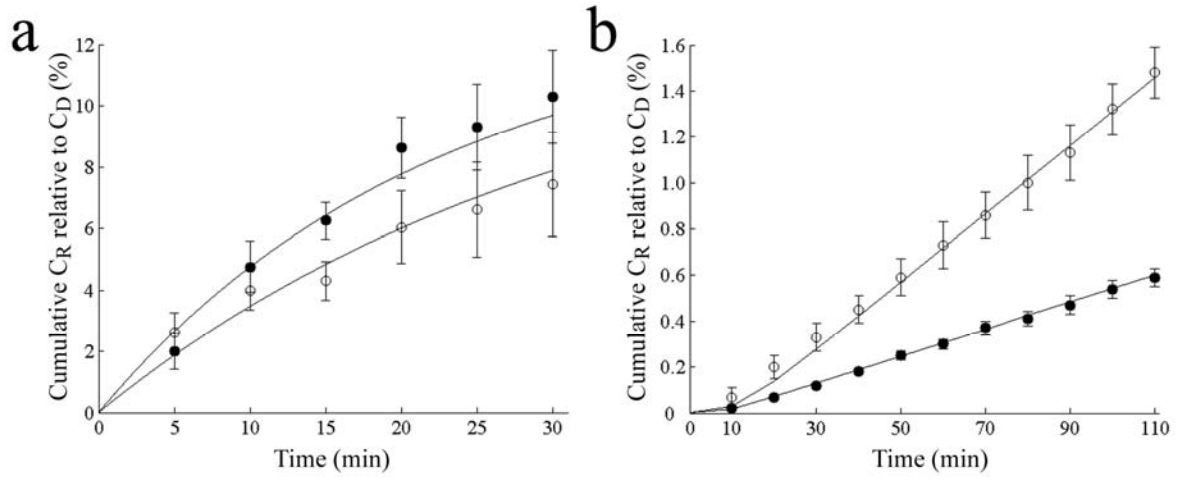

Figure 7 Transport kinetics of [^{14}C]-sucrose (o) and [^{3}H]-vinblastine (●) was determined through (a) Transwel-Col membranes and (b) MCL. Typically 800 nM [^{14}C]-sucrose or 60 nM [^{3}H]-vinblastine was administered to the DC. Appearance of radiolabelled compound in the RC was measured as described in *Materials and Methods*. The cumulative concentration in the receiver compartment (C_R) was divided by the starting concentration in the donor compartment (C_D) and plotted as the mean percentage ± SD of three independent experiments. The curves were fitted using the mathematical models described in the *Appendix*.

Similarly to sucrose, the flux rate of vinblastine through the MCL was significantly slower than that observed through the PTFE membrane alone (Fig. 7a & b). Vinblastine is lipophilic and its distribution was expected to include the intracellular space in MCL. Surprisingly, the mathematical model that was based purely on diffusion, *i.e.* without any reaction term, described the flux of vinblastine through MCL accurately (Fig. 7b). On the other hand, the measured radioactivity in the RC can represent both vinblastine and its metabolites and thus it can overestimate the flux of the parental compound. However, there wasn't any Cyp3A4, which is the major metabolising enzyme of vinblastine *in vivo,* detected in the MCL with western immunoblotting techniques (data not shown). The measured diffusivity of [^{3}H]-vinblastine through the DLD1 MCL was $1.9 \pm 0.2 \times 10^{-8}$ cm^2 s^{-1}. The diffusivities of both compounds decreased approximately 170 fold in the MCL compared to the medium, so the MCL hindered the diffusion of vinblastine to the same extent as it did for sucrose.

In summary, the drug transport assay presented here consists of two compartments separated by a MCL with heterogeneous cell populations and low/moderate P-gp expression. Both [^{3}H]-vinblastine and [^{14}C]-sucrose fluxes were compatible with pure extracellular diffusion and [^{3}H]-vinblastine diffusivity was more than two fold slower in the MCL. Due to its slow diffusivity, vinblastine will mostly affect cells nearer than 70 μm to the vessel wall.

4.2.3. Diffusivity and cellular uptake rate of [^{14}C]-Pt(II) and [^{14}C]-Pt(IV) compounds in MCL

The transport of the compounds through the PTFE membrane with or without the MCL was measured by loading the radiolabelled drugs to the DC and measuring the radioactivity appearing in the RC over time (Figure 2a). Initially, 150 and 1000 μL volumes of culture medium were loaded to the DC and RC respectively, to maintain an equivalent fluid level and therefore avoid hydrostatic pressure driven convective transport.

The non-specific binding of the compounds to the plastic surfaces in DC and RC was determined to improve the accuracy of the subsequent quantitative analyses (Table 2). For example, the fraction bound to the DC reduces the effective concentration gradient, whilst the fraction bound to the RC falsely reduces the flux rate. The fractions bound to the DC and to the RC were used to correct the starting drug concentration and the concentration of the drug transported respectively. The cumulative concentration of [^{14}C]-Pt(II) and [^{14}C]-Pt(IV) were expressed as a percentage of the initial drug concentration in the DC.

Table 2 Binding of the radiolabelled compounds in the MCL system

%, mean ± SD	Membrane		MCL	
	[^{14}C]-Pt(II)	[^{14}C]-Pt(IV)	[^{14}C]-Pt(II)	[^{14}C]-Pt(IV)
Added to DC	100	100	100	100
Decrease in DC	46.3 ± 2.6 n = 3	43.06 ± 2.6 n = 3	17.6 ± 3.6 n = 12	15.3 ± 4.1 n = 12
Membrane ± MCL	0.1 ± 0.1 n = 3	0.3 ± 0.1 n = 5	0.7 ± 0.3* n = 6	0.5 ± 0.2* n = 9
Transported	27.8 ± 5.0 n = 3	28.6 ± 3.5 n = 3	5.3 ± 0.8 n = 12	5.3 ± 0.5 n = 12
Bound to RC	12.8 ± 0.4 n=3	16.6 ± 1.2 n = 3	12.8 ± 0.4 n=3	16.6 ± 1.2 n = 3
Bound to DC	18.5 ± 7.0 n = 3	13.9 ± 5.6 n = 3	10.1 ± 2.8 n = 6	10.5 ± 4.3 n = 9

The percentage bound to the DC was calculated by subtracting the percentage bound to membrane ± MCL and the percentage transported to the RC from the percentage decrease in the DC at the end of the transport assay. These values and the non-specific binding of radiolabelled compounds to the RC were measured as it is described in Materials and Methods. * indicates statistically significant ($p < 0.05$) accumulation of the Pt compounds in the MCL compared to the PTFE membrane alone.

Figure 8 shows the cumulative amounts of Pt-complexes appearing in the DC of the MCL apparatus. Data is provided for fluxes in the presence or absence of the MCL tissue overlaid on the PTFE membrane. As expected, the rate and extent of flux was greater for both drugs in the absence of the MCL. The data in Figure 8 clearly demonstrates that there was no difference between [^{14}C]-Pt(IV) and [^{14}C]-Pt(II) with respect to their cumulative appearance in the donor compartment.

Mathematical modelling without a cellular uptake parameter did not fit the data obtained in the presence of an MCL, but was an accurate reflection for passage across the PTFE membrane alone. The mathematical model comprising an uptake coefficient was used to quantify flux of the compounds through the solid tumour model and the data is summarised in Table 1.

Figure 8 Flux kinetics of [^{14}C]-Pt(II) and [^{14}C]-[Pt(IV) through MCL

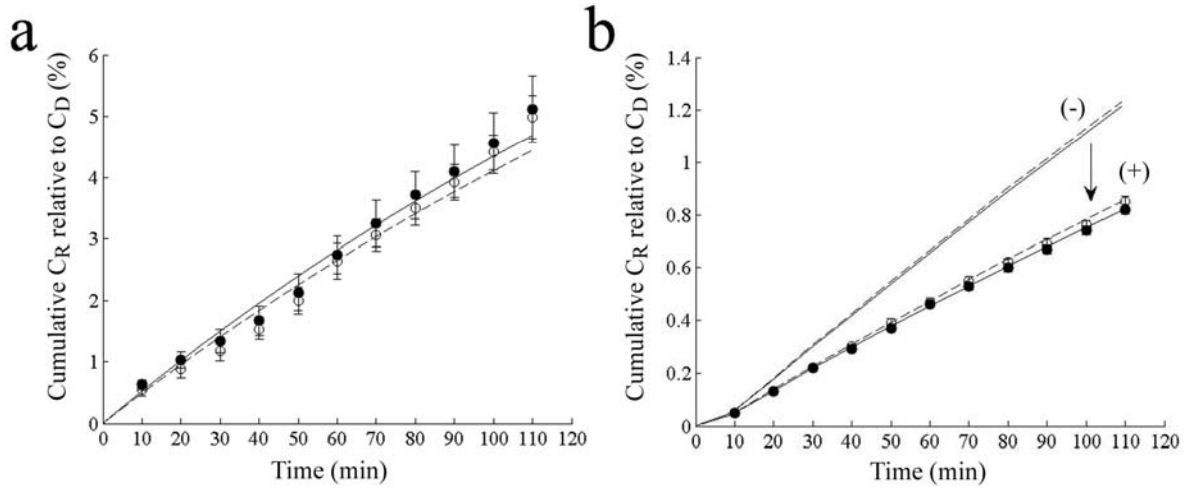

Typically, concentrations of 6 μM [^{14}C]-Pt(II) (●) and 18 μM [^{14}C]-Pt(IV) (o) were administered to the DC. Appearance of radiolabelled compound in the RC was measured as described in *Materials and Methods*. The cumulative concentration in the receiver compartment (C_R) was divided by the starting concentration in the donor compartment (C_D) and plotted as the mean percentage ± SD of three independent experiments. The curves were fitted using the mathematical models with (+) or without (-) terms for cellular uptake as described in the *Materials & Methods*. Flux was measured through (a) the PFTE membrane only and (b) MCL grown on the PFTE membrane.

The D_c of platinum compounds in solution was calculated according to the Stokes-Einstein equation (Eq. 1) using the molecular radius (MR). The mass transfer coefficients (k) and relative porosity (ψ) values of the two platinum compounds through MCLs were indistinguishable. The coefficient of diffusion was ascertained for the Pt(IV) and Pt(II) drugs through the MCL model utilising the parameters of mass transfer coefficient (k), MCL thickness (x_M), diffusivity in the medium (D_1) and initial drug concentration (C_D). The calculated diffusion coefficients (D_M) and cellular uptake (g) rates were not different for the two platinum compounds (Table 1), reflecting similar flux parameters for the two classes of platinum complex in a solid tissue.

4.2.4. Cellular accumulation of [^{14}C]-Pt in the MCL; SRIXE Analysis

Accumulation of Pt compounds in the MCL was determined by measuring the radioactivity retained in the PTFE membrane ± MCL after the transport assays. As shown in Table 2, the radioactivity associated with the membrane was higher in the presence of the MCL, although there was no significant difference between [^{14}C]-Pt(II) compared to [^{14}C]-Pt(IV).

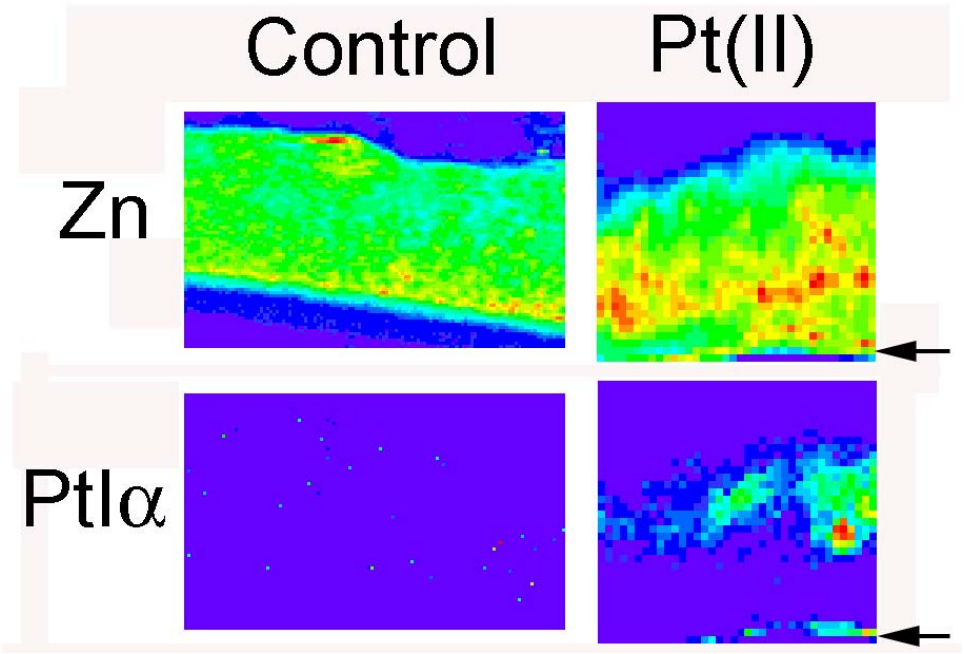

Figure 9 The cellular accumulation of [^{14}C]-Pt(IV) in MCL: SRIXE analysis

After the transport assay sections of the MCL were imaged using SRIXE. Fitted images of the elemental distributions in segments of a control and a Pt(IV) treated MCL are shown, where each pixel represents 3 x 2 μm (horizontal x vertical). The images show relative elemental concentrations on blue to red colour scale, representing low to high elemental levels. The arrowheads indicate the position of the PTFE membrane supporting the MCL.

Data from the mathematical modelling above suggested a significant degree of uptake for Pt-drugs within the MCL tissue. Image analysis using SRIXE was used to confirm this suggestion and the technique enabled an extensive elemental analysis of the MCL tissue. The data shows that tissue that had been exposed to the [^{14}C]-Pt(IV) drug was associated with an incorporated Pt-signal (Figure 9). This confirmed the experimental and mathematical modelling data and demonstrates that flux through solid tissue is associated with a non-negligible degree of Pt-drug uptake into cells. Quantitation of the Pt signal across the tissue

revealed a greater Pt(IV)-complex concentration at the upper surface (*i.e.* facing the DC) (Figure 10).

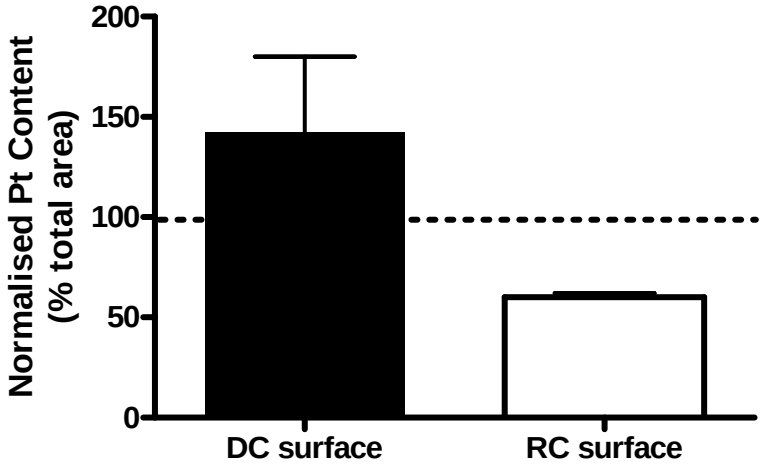

Figure 10 Quantification of the cellular accumulation of [^{14}C]-Pt(IV) in MCL

The platinum contents of the surfaces exposed to the DC and the RC were quantified and normalised relative to a region representative of the entire MCL. Values are expressed as percentages, where a value of 100 is indicative of an elemental content identical to that of the whole MCL. The data represent the mean and standard error associated with two scans.

4.2.5. The effect of hydrostatic pressure on the flux of [^{14}C]-Pt(IV) through MCL

The six-coordinate Pt(IV) compounds have been proposed to display a greater likelihood of reduction to the active Pt(II) species in the hostile intra-tumour micro-environment. Consequently, ensuring sufficient penetration of Pt(IV) drugs to the deeper layers of a tumour remains a key issue. One proposed way of improving penetration is to increase the hydrostatic pressure to counteract the increased interstitial pressure generated in tumours. The MCL system (Figure 2a-c) provides a convenient means to investigate whether hydrostatic pressure can modulate the flux of [^{14}C]-Pt(IV) through solid tumour tissue. Hydrostatic pressure may be varied by simply altering the fluid levels in the DC and RC and was applied in both the same and opposite directions to the concentration gradient of the MCL system. Figure 11 shows the cumulative amount of [^{14}C]-Pt(IV) that had penetrated through the MCL in to the lower RC, relative to the amount of drug added originally to the DC.

Figure 11 The effect of hydrostatic pressure on flux kinetics in MCL

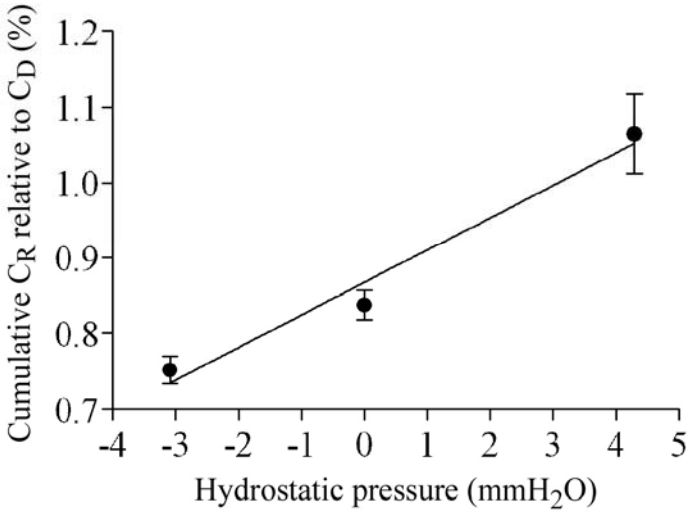

Hydrostatic pressure was applied by varying the volume of medium added to the DC and the RC as described in *Materials and Methods*. The flux kinetics [^{14}C]-Pt(IV) were determined and the cumulative RC concentration relative to the diffusion only values are shown as mean ± SEM of at least 3 independent experiments.

At a hydrostatic pressure of -3 mm H_2O (i.e. against concentration gradient) the amount of penetration was reduced from 0.82±0.01% to 0.73±0.01%. In contrast, as the hydrostatic pressure was increased to +4 mm H_2O (*i.e.* along the concentration gradient), the flux of [^{14}C]-Pt(IV) was increased to 1.06±0.08%. The data therefore indicates that even a relatively minor hydrostatic pressure gradient was capable of a significant influence on the flux of [^{14}C]-Pt(IV) through the MCL tumour model.

4.3. Diffusion of vinblastine in a cylindrical model system of colon cancer tissue

Vinblastine is administered IV to patients and it is delivered by the blood to the cancer tissue. Blood vessels can be considered as tubes and drug enters tissues in all radial directions from the vessels To mimic this situation we designed a model system with radial symmetry from blood vessels running parallel to each other and assuming that the surrounding space was filled with colon cancer tissue with the same cell volume fraction and impedance as in the MCL.

Figure 12 Vinblastine concentration profiles in colon cancer tissue

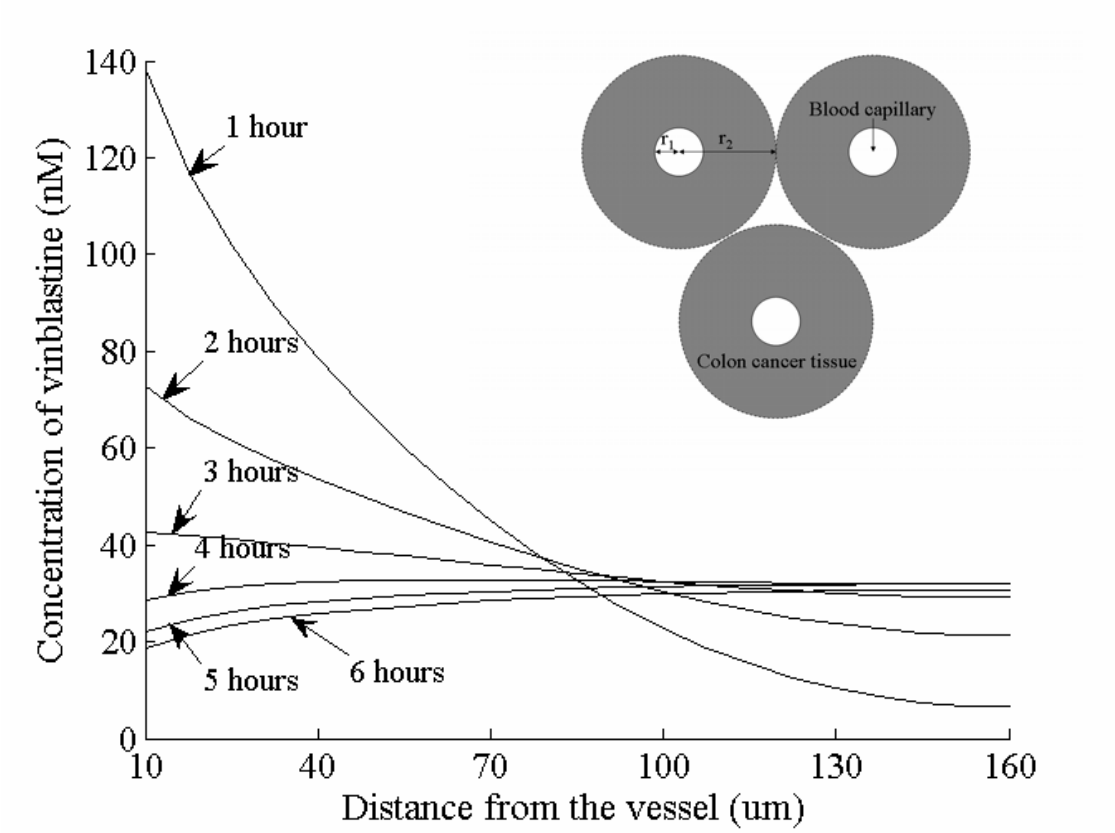

Vinblastine distribution was modelled in cylindrical system with 160 μm radius (r_1+ r_2) and a central vessel that has a radius of 10 μm (r_1), as it is show in the insert. The vinblastine concentration in the vessel was changing according to observed profiles after a short infusion of a single dose of the drug [49]. The graph shows successive predicted profiles at one hour intervals using the measured diffusivity of vinblastine. The mathematical model used to predict tissue drug concentrations is detailed in the *Appendix*.

The distance between two vessels represents the average intercapillary distance in tumours [8]. A cross section of this model is shown in the insert of Figure 12. The tissue distribution of vinblastine was estimated after a single dose of the drug with blood concentration decreasing according to a four compartment model [49]. In this model the 70 μm ring of cancer tissue proximal to the vessel wall will experience the highest exposure to vinblastine, while tissues further away will be relatively spared (Figure 12).

5. Discussion

5.1. The MCL as an experimental model system

In this study we aimed to provide a model for investigating kinetics of chemotherapeutic drug flux in solid tumour nodules. A three-dimensional cancer tissue model (*i.e.* multicell layer) was reproducibly cultured from DLD1 colon cancer cells. The MCL system is widely accepted as a good model of solid tumour tissue, in particular the non-vascularised regions or nodules [50-51].

The experimental model coupled with mathematical analysis presented here proved suitable for measuring the diffusivity of chemotherapeutics in cancer tissue. The MCL grown from DLD1 colon cancer cells recapture many key features of colon adenocarcinoma, *e.g.* cellular morphology and severe dysplasia [52]. Furthermore, MCLs display heterogeneity of cell cycle status (*i.e.* proliferating and quiescent) in addition to having a high cell density and localised regions of hypoxia, which are common features of many solid tumours.

The applied mathematical model requires that the MCL retain their architecture and cell viability during the experiment. The duration of the flux assay was significantly shorter than the doubling time of DLD1 cells in monolayer cultures (34 hours, data not shown) and the estimated time required by a cell to undergo apoptosis (12-24 hours, [53]). Hence, we can assume that there was neither significant proliferation nor cell loss during the experiment.

In order to exclusively measure diffusion, the experimental conditions should exclude convection due to a temperature gradient or hydrostatic pressure. To ensure this, the experiments were conducted in an incubator and the fluids in the donor and receiver compartments were kept at the same level, unless otherwise specified.

This experimental set-up was validated by measuring the flux of [^{14}C]-sucrose, which is neither taken up nor metabolised in the MCL. The mathematical model based on Fickian diffusion was able to describe the sucrose flux through the MCL. Thus, the presented transport assay is suitable to measure the diffusivity of various compounds through the

extracellular space of the MCL and deviations of the flux from the diffusion based mathematical model could signal the interaction of the drug with the tumour tissue.

5.2. Transport of the ABCB1 substrate vinblastine

Sucrose flux through the MCL was expected to show exclusively extracellular diffusion kinetics and, indeed, it was accurately described by the Fickian diffusion model. Although, the flux of vinblastine through MCL was considerably slower than sucrose, it was compatible with extracellular diffusion. The tissue distribution profile based on the diffusivity of vinblastine predicted that cells up to 70 μm away from the circulation will get the highest exposure to the drug.

The flux of vinblastine through the MCL was accurately described by the Fickian diffusion model suggesting that vinblastine was not metabolised or taken up by cells in this system. Vinblastine, which is a lipophilic compound, was expected to enter cells and that its flux through the MCL will deviate from Fickian diffusion. However, vinblastine is also a substrate of multidrug ABC transporters, which are expressed in colon cancer cells. We've found that P-gp is expressed at levels intermediate between parental and drug selected cell lines and P-gp in DLD1 MCL may have restricted vinblastine distribution to the extracellular space.

This is the first report that provides a quantitative measure for the actual diffusion coefficient of vinblastine in 3-D tumour tissue models. To date there are only a few data available about drug diffusivity in tumor tissue models and our results are in the same range that has been reported previously (Table 3).

Table 3 Examples of drug diffusivities in MLCs

Drug	**Molecular mass (g/mol)**	**D_c in tumour tissue (x 10^{-7} cm^2s^{-1})**
[^{14}C]-urea [13]	60	14.5
Misonidazole [54]	201	5.5
Tirapazamine [55]	178	4.0

The penetration of vinblastine through MCL has been reported previously [7]. However, kinetic parameters of penetration such as $T_{1/2}$ are not constants and therefore dependent on specific experimental conditions. Furthermore, penetration depends not only on the diffusivity of a compound, but also on the hydraulic conductance of the tissue if there is any convection

[56]. In addition, penetration can be further diminished by extensive cellular uptake, metabolism or binding to specific receptors. We have demonstrated that the diffusion of vinblastine was app. 170 times slower in tumour tissue than in solution and 2.5 fold slower than that of sucrose.

Which components of the extracellular space in the MCL play a role in limiting vinblastine diffusion? The presence of extracellular matrix in 3-D tumour models could increase the exerted hindrance (i.e. impedance) of the tissue and should be proportional to the size of molecules [57]. However, experimental results do not support a strict correlation between molecular size and diffusivity in tissues [58]. Similarly, in this study the impedance of the MCL was equal for sucrose and vinblastine, despite the fact that their respective molecular radii are different. It is possible that the geometry of the extracellular space is responsible for slowing down diffusion of solutes in tissues. To further specify, based on mathematical models Tao and Nicholson concluded that impedance is not dependent on cell shape but on the relative volume of the extracellular space [59]. These findings emphasise the role of tight cell packing and intercellular contacts as limiting factors of transport in the interstitium. Thus, it is necessary to dissect flux data, as flux through the 3D model membrane is a sum of many different processes.

Would it be beneficial to somehow increase the flux of vinblastine in tumour tissues? Vinblastine penetration into tissues with high interstitial pressure will be poor and it will likely to reach cells only in the vicinity of blood vessels. Previously the efficacy of vincristine was correlated with the proliferating population of cells in monolayers, TS and tumour xenografts [60]. Furthermore, we have shown that quiescent cells are insensitive to vinblastine in a modified TS model (manuscript # IV.). The mitotically active cells in solid tumours reside in close proximity to capillaries and even slowly diffusing vinblastine can penetrate to sufficient depth to reach those cells. On the other hand, cells further away from the circulation are not sensitive to vinblastine, hence increased penetration of vinblastine is unlikely to improve therapeutic efficacy. Drug distribution and target cell populations should ideally overlap in tumours and the MCL model can be used to identify drugs that fall short of this requirement.

5.3. Transport of platinum compounds

Platinum based chemotherapy remains a vital component of many treatment strategies in oncology. As with the majority of "genotoxic" anticancer drugs, the Pt-complexes are beset by problems with toxicity, resistance and poor pharmacokinetic properties. A great deal of effort has been placed in generating more potent and selective derivatives of conventional Pt(II) drugs such as cisplatin. In particular, the six coordinate Pt(IV) complexes offer several advantages including lower reactivity and a greater potential for introducing hydrophobicity to facilitate cellular uptake. There is little information available on either class of Pt-drug relating to their behaviour in solid tumour tissue, so the MCL as solid tumour model was utilised to quantify flux behaviour of Pt(II) and Pt(IV)-complexes. Flux through the solid tumour model was associated with significant cellular accumulation and was sensitive to changes in the applied hydrostatic pressure.

Both of the compounds tested were able to completely penetrate the MCL tissue with the diffusion coefficients of $17.5 \pm 2.6*10^{-8}$ cm^2s^{-1} for the Pt(II) and $17.8 \pm 3.1*10^{-8}$ cm^2s^{-1} for the Pt(IV)-complex. These rates of diffusion were almost ten fold higher than that for the hydrophobic anticancer drug vinblastine ($1.9 \pm 0.2*10^{-8}$ cm^2s^{-1}) and four fold higher than of the highly hydrophilic sucrose ($4.2 \pm 0.9*10^{-8}$ cm^2s^{-1}). A similar rapid flux (*i.e.* % drug min^{-1}) of cisplatin compared to vinblastine has been reported in MCL comprising bladder cancer cells, whilst etoposide, gemcitabine and paclitaxel displayed faster rates of flux [7]. A major advantage of the current approach is the ability to estimate the actual diffusion coefficients, which may be directly applied to the prediction of tissue drug concentrations; for example, as a function of the distance from a blood vessel (Fig. 12). This rapid flux across the MCL should be considered a positive feature for such compounds. A considerable emphasis in the design of platinum drugs has been placed on developing lipophilic drugs that can assist in circumventing diminished cisplatin accumulation in resistant cell lines, however it may be that defeating unicellular resistance may come at the expense of tissue penetration, and therefore create the problem of multicellular resistance. It seems that hydrophilic drugs such as those examined here allow for excellent tissue penetration. If this feature can be coupled with a more readily reducible Pt(IV) compound (the Pt(IV) compound studied here is the most inert in a series studied), a drug with good penetration and cytotoxic potential may be arrived at.

The idea of improving cell penetration and nuclear targeting at the same time by adding an anthraquinone moiety to the Pt(II) backbone (Pt-1C3) was explored (manuscript # V). Pt-1C3 and 1C3 alone had similar IC_{50}'s and were more potent than cisplatin in citotoxicity assays with DLD1 cells. However, confocal microscopy revealed that Pt-1C3 was sequestered in the lysosomes and spared the nucleus. Similar discouraging results were published about the dinuclear anthraquinone modified Pt drug tested on drug resistant A2780 cells [67].

The Pt(IV) compound used in the present study has been shown to display lower cellular accumulation in well oxygenated monolayers of cancer cells [32] and lower serum protein binding compared to the Pt(II) parental derivative [28]. Therefore Pt(IV) would be expected to display higher flux rates across MCL than Pt(II); unless the compound is rapidly converted to the parental Pt(II) version. The latter is highly unlikely since even following a 24 hour incubation period in cancer cells detection with micro-XANES revealed that the Pt(IV)-complex was not significantly reduced to the four coordinate form [61]. The two Pt compounds had undistinguishable flux kinetics across the MCL and in both cases the mathematical model required the inclusion of a specific component to account for cellular uptake within the tissue. Similarly, the calculated diffusion constants and cellular uptake rates also failed to detect any pharmacokinetic differences between the two compounds. What is the explanation for the similar rates of flux through the solid tissue given the physico-chemical differences between Pt(II) and Pt(IV) species? Perhaps despite the increased propensity to cross membranes, the accumulation of [^{14}C]-*cis,trans*-[$PtCl_2(OH)_2$(en)] is limited by the lack of reactivity. For example, if the latter was more reactive and thus converted to the corresponding Pt(II) compound the concentration gradient into the cell for the Pt(IV) would remain high enough to ensure greater uptake. Consequently, future Pt(IV) development would require taking into account both transbilayer diffusion and the intracellular reactivity.

In addition to allowing detailed flux analysis, the mathematical model predicts that a concentration gradient would exist within the MCL decreasing from the free surface of the tissue towards the semiporous PTFE membrane (*i.e.* DC→RC direction). The SRIXE element array qualitatively demonstrated that the distribution of the Pt(IV) compound was similar to that predicted by the mathematical model, *i.e.* more Pt was detected close to the free surface of the MCL. This is the first report, where the distribution of drugs within the MCL was experimentally verified and compared to the one predicted by mathematical modelling. That

more Pt was observed close to the upper surface of the MCL is in keeping with previous observations with cisplatin detected by antibody in squamous carcinoma cell spheroids, and a Pt-porphyrin compound in J82 spheroids observed by fluorescence microscopy that inferred more intense drug signal (though both relied on a molecular signature other than the active Pt centre itself) at the periphery of spheroids [62-63]. In the case of the Pt-porphyrin complex, it took 24 hours before uniform drug distribution could be achieved, though this is not reflective of the drug distribution expected to be achieved by a pulse of chemotherapeutic agent. SRIXE assay enabled direct quantification of Pt(II) and Pt(IV) distribution within tumour cell spheroids. Both compounds showed similar distribution, *i.e.* being more abundant at the periphery of the spheroid and less so in the middle region (manuscript # VI.). These results are in line with results from MCL experiments showing a steep downwards gradient of Pt content going from the surface to the middle of the MCL.

Most solid tumours have high interstitial pressures that slow drug transit and filtration through tissue and consequently drug movement in cancer tissue is largely limited to diffusion [10]. Restoring the physiological filtration by increasing the hydrostatic pressure is a possible option to improve drug delivery to deeper layers of cancer cells within the 3-dimensional solid tumour mass. Our results show that since the flux of the two compounds was sensitive to hydrostatic pressure that convection could potentially increase the penetration of tumour mass by platinum drugs. This principle, known as convection enhanced delivery (CED), has actually been utilised to treat intracranial tumours where the confined space further increases the effects of interstitial pressure [64]. Cisplatin is expected to be useful via local drug delivery [65] in intracranial tumours due to its reported rapid flux rate, although an enhancement by CED has not yet been examined.

The data from the present investigation provides hitherto unknown pharmacokinetic properties for two platinum compounds; namely the absolute diffusion coefficient through solid tumour tissue. Moreover, both experimental and mathematical models provide a convenient means to facilitate the *in vitro* development of novel six-coordinate platinum compounds; particularly to enable a bridge between observations in simple cell monolayer systems to the complexities associated with poorly vascularised hypoxic tumours *in vivo*.

6. Summary

The three-dimensional organisation of cancer cells in solid tumours contributes to the multi-factorial problem of drug resistance. Impaired diffusion through tumour tissue is often thought as a major contributing factor in resistance, yet elucidating intra-tumoural distribution of anti-cancer drugs is often neglected.

Our approach to these problems was to develop tools that can help to estimate drug distribution in vivo. 3-D tumour models were selected to serve as model systems and drug transport was measured in these models. A mathematical model was developed to describe the distribution of anti-cancer drugs through solid tumour tissue. The flux of various compounds was measured through the multicell layer tumour model comprising DLD1 colon cancer cells. Fluxes were determined for sucrose, vinblastine and [^{14}C]-labelled [$PtCl_2$(en)] and cis,trans-[$PtCl_2(OH)_2$(en)] drugs. The mathematical model provided the diffusion coefficients for these compounds and together with experimental data it suggested a significant cellular uptake of the platinum compounds in the transport system.

Although slow diffusion delays vinblastine penetration into the avascular regions of tumours, the proliferating cells susceptible to mitotic spindle poisons are generally in the perivascular area of tumours. The flux of the Pt(IV) compound through the MCL was not significantly different to that of the Pt(II)-drug nor were the diffusion coefficient or tissue uptake; the latter confirmed with elemental imaging analysis by synchrotron radiation induced X-ray emission. However, the flux of the Pt(IV) through the MCL was increased by hydrostatic pressure, thereby demonstrating the potential to target cancer cells further away from the vessels with six-coordinate platinum drugs.

The experimental and mathematical model described has broad applicability for the study of anticancer drug diffusion in 3-D tumour tissue. The mathematical model enables accurate quantification of drug pharmacokinetic behaviour within solid tissue and may be adapted to incorporate the influence of factors mediating pharmacokinetic drug resistance. Determination of the diffusivity of chemotherapeutic agents can help to identify compounds with potential in pharmacokinetic drug development.

7. Appendix

7.1. Mathematical model to describe drug flux through Transwell-Col membranes only

The experimental system is depicted in Figure 2 and is modelled as a closed system with mass conservation:

$$V_D C_{D_0} = V_D C_D(t) + V_R C_R(t), \qquad \text{(Equation 2)}$$

where V_D and V_R are the volumes of the donor and receiver compartments (mL), respectively, and C_{Do} is the initial concentration of the radiolabelled compound in the donor chamber (nM), while $C_B(0) = 0$ nM. The flux through the membrane is proportional to the membrane surface area (A, cm^2) and the concentration gradient across the membrane. Furthermore the flux through the membrane equals the change of concentration of molecules in the receiver compartment, hence we get

$$\frac{d}{dt} C_R(t) = \frac{Ak}{V_R}\left(C_D(t) - C_R(t)\right), \qquad \text{(Equation 3)}$$

where k is the mass transfer coefficient (cm s^{-1}). C_D can be eliminated using Eq. 1 and then Eq. 2 solved:

$$C_R(t) = \frac{V_D C_{D_0}}{V_R + V_D}\left(1 - e^{-\frac{Ak}{V_R}\left(\frac{V_R}{V_D}+1\right)t}\right). \qquad \text{(Equation 4)}$$

The fitted parameter was k and the relative porosity of the membrane for the compounds (~impedance, ψ) was determined according to

$$k = \frac{D_1 \psi}{\Delta x}, \qquad \text{(Equation 5)}$$

where D_1 is the diffusion coefficient of the compound in medium ($cm^2 s^{-1}$) and Δx is the measured thickness of the membrane (cm). This model assumes that the non-specific binding of compounds to the membrane is negligible.

7.2. Mathematical model to describe flux of radiolabelled compounds through the MCL and the membrane

The flux of radiolabelled compounds through the MCL was modelled as Fickian diffusion. As we described previously the MCL resembles the heterogeneity of solid tumours. However, in MCL this heterogeneity appears in planes perpendicular to the axis of the drug concentration gradient and thus the insert with the MCL can be seen as an anisotropic cylinder which has its

axis along direction x (Fig. 2) and is bounded by planes perpendicular to x and the problem of diffusion into it reduces to the corresponding problem in an isotropic cylinder provided $D_y = D_z$, where D_y and D_z are diffusion constants in the other two directions of space [66]. The concentration of compounds in the donor compartment was kept constant during the experiment. As the concentration only varies along the x axis we can describe the diffusion as

$$\frac{\partial c}{\partial t} = \frac{\partial}{\partial x}\left(D_M \frac{\partial c}{\partial x} \right), \qquad \text{(Equation 6)}$$

where D_M is the diffusion coefficient of the compound in the MCL ($cm^2\ s^{-1}$) and x is the distance from the top free surface of the MCL (cm). D_M can be defined by the impedance of MCL (Γ) and the diffusivity of the compound in medium (D_1, $cm^2\ s^{-1}$) as

$$D_M = \Gamma * D_1 \qquad \text{(Equation 7).}$$

The boundary conditions were

at $x = 0$ $\qquad C(0,t) = C_{D_0}$,

for the continuity of the flux at the interface between the MCL and the membrane

at $x = x_M$ $\qquad -D_M \frac{\partial}{\partial x} C(x_M, t) = k\left(C(x_M, t) - C_R(t)\right)$, $\qquad$ (Equation 8)

where x_M is the thickness of the MCL. Furthermore the governing equation for the drug concentration in the RC ($C_R(t)$) is

at $x = x_M$ $\qquad \frac{d}{dt} C_R(t) = \frac{Ak}{V_R}\left(C(x_R, t) - C_R(t)\right)$. $\qquad$ (Equation 9)

Eq. 7 and 8 are coupled partial differential equations, which were used to write a program in Matlab 7.0.1 to simulate the experimental situation with initial conditions $C(x,0) = C_{D_0}$ at $x = 0$, $C(x,0) = 0$ at $0 < x \le x_M$ and $C_R(0) = 0$ to calculate Γ and D_M.

7.3. Mathematical modelling of vinblastine distribution in colon cancer tissue with radial symmetry

The model system consists of capillaries running parallel to each other and surrounding colon cancer tissue. A cross section of this system is shown in the insert on Figure 12. To describe the distribution of vinblastine after a single dose from the central vessel into the surrounding cancer tissue we used the following equation:

$$\frac{\partial c}{\partial t} = \frac{1}{r}\frac{\partial}{\partial r}\left(D_M r \frac{\partial c}{\partial r} \right), \qquad r_1 < r < r_2 \qquad \text{(Equation 10)}$$

The boundary conditions were

at $r = r_1$ $\quad c(r_1, t) = \sigma(t)$

and at $r = r_2$ $\quad \frac{\partial}{\partial r} c(r_2, t) = 0$.

The initial conditions were

at $r = r_1$ $\quad c(r,0) = \sigma_0$

and at $r_1 < r < r_2$ $\quad c(r,0) = 0$.

Equation 9 was solved numerically and tissue drug concentrations were plotted against distance from the centre of the vessel in Figure 12. Metabolism was considered to be negligible and we kept the cell volume fraction constant. However, applying the measured proliferation rate constant and literature values for apoptotic cell death rate and tissue metabolism did not influence the drug distribution in the first 6 hours.

7.4. Mathematical Model to Describe Intra-MCL Drug Pharmacokinetics

Transport through the Transwell-Col membrane only was described using the model and equations detailed in chapter 6.1.

The transport of radiolabelled platinum compounds through the MCL was using a modified version of the model described in chapter 6.2, i.e. included another term to account for cellular uptake. As the concentration only varies along the x axis we can describe the diffusion of the drug in the MCL by

$$\frac{\partial c}{\partial t} = \frac{\partial}{\partial x}\left(D_M \frac{\partial c}{\partial x} \right) - g * \phi * c \,, \qquad \text{(Equation 11)}$$

where D_M is the diffusion coefficient of the compound in the MCL ($cm^2\ s^{-1}$) and x is the distance from the top free surface of the MCL (cm), and g (s^{-1}) is the rate of cellular uptake of the compound, ϕ is the cell volume fraction and c (nM) is the drug concentration.. D_M can be defined by the impedance of MCL (Γ) and the diffusivity of the compound in medium (D_1, $cm^2\ s^{-1}$) as

$$D_M = \Gamma * D_1 \qquad \text{(Equation 12).}$$

The boundary conditions were

at $x = 0$ $\quad C(0,t) = C_D(t)$,

Where the concentration in top compartment is calculated from the mass balance by considering the flux of molecules that enters the MCL, *i.e.*

$$\frac{d}{dt}C_D(t) = \frac{AD}{V_D}\frac{\partial c}{\partial x}\bigg|_{x=0} \quad \text{with initial condition } C_D(t=0) = C_{D_0}. \qquad \text{(Equation 13)}$$

The continuity of the flux at the interface between the MCL and the membrane gives us another boundary condition

$$\text{at } x = x_M \qquad -D_M \frac{\partial}{\partial x}C(x_M, t) = k\left(C(x_M, t) - C_R(t)\right), \qquad \text{(Equation 14)}$$

where x_M is the thickness of the MCL. Furthermore the governing equation for the drug concentration in the RC ($C_R(t)$) is

$$\text{at } x = x_M + \Delta x \qquad \frac{d}{dt}C_R(t) = \frac{Ak}{V_R}\left(C(x_R, t) - C_R(t)\right). \qquad \text{(Equation 15)}$$

Eq. 10-14 are coupled partial differential equations, which were used to write a program in Matlab to simulate the experimental situation with initial conditions $C = 0$ at $0 < x \le x_M$ and $C_R(0) = 0$ to calculate Γ, D_M and g.

8. References

1. Modok S, Mellor HR, Callaghan R. Modulation of multidrug resistance efflux pump activity to overcome chemoresistance in cancer. Curr Opin Pharmacol. 2006 Aug;6(4):350-4.

2. Storm J, Modok S, O'Mara ML, Tieleman DP, Kerr ID, Callaghan R. Cytosolic region of TM6 in P-glycoprotein: topographical analysis and functional perturbation by site directed labeling. Biochemistry. 2008 Mar 25;47(12):3615-24.

3. McDevitt CA, Collins RF, Conway M, Modok S, Storm J, Kerr ID, Ford RC, Callaghan R. Purification and 3D structural analysis of oligomeric human multidrug transporter ABCG2. Structure. 2006 Nov;14(11):1623-32.

4. Rosenberg MF, Callaghan R, Modok S, Higgins CF, Ford RC. Three-dimensional structure of P-glycoprotein: the transmembrane regions adopt an asymmetric configuration in the nucleotide-bound state. J Biol Chem. 2005 Jan 28;280(4):2857-62.

5. Modok S, Heyward C, Callaghan R. P-glycoprotein retains function when reconstituted into a sphingolipid- and cholesterol-rich environment. J Lipid Res. 2004 Oct;45(10):1910-8.

6. Desoize B. & Jardillier J. (2000). Multicellular resistance: a paradigm for clinical resistance? *Crit Rev Oncol Hematol*, **36,** 193-207.

7. Tannock I.F., Lee C.M., Tunggal J.K., Cowan D.S. & Egorin M.J. (2002). Limited penetration of anticancer drugs through tumor tissue: a potential cause of resistance of solid tumors to chemotherapy. *Clin Cancer Res*, **8,** 878-84.

8. Konerding M.A., Fait E. & Gaumann A. (2001). 3D microvascular architecture of pre-cancerous lesions and invasive carcinomas of the colon. *Br J Cancer*, **84,** 1354-62.

9. Tong R.T., Boucher Y., Kozin S.V., Winkler F., Hicklin D.J. & Jain R.K. (2004). Vascular normalization by vascular endothelial growth factor receptor 2 blockade induces a pressure gradient across the vasculature and improves drug penetration in tumors. *Cancer Res*, **64,** 3731-6.

10. Heldin C.H., Rurin K., Pietras K. & Ostman A. (2004). High interstitial fluid pressure - an obstacle in cancer therapy. *Nat Rev Cancer*, **4,** 806-13.

11. Durnad R.E. (1990). Slow penetration of anthracyclines into spheroids and tumors: a therapeutic advantage? *Cancer Chemother Pharmacol*, **26,** 198-204.

12. Martin C., Walker J., Rothnie A. & Callaghan R. (2003). The expression of P-glycoprotein does influence the distribution of novel fluorescent compounds in solid tumour models. *Br J Cancer*, **89,** 1581-9.

13. Hicks K.O., Ohms S.J., van Zijl P.L., Denny W.A., Hunter P.J. & Wilson W.R. (1997). An experimental and mathematical model for the extravascular transport of a DNA intercalator in tumours. *Br J Cancer*, **76,** 894-903.

14. Hicks K.O., Pruijn F.B., Sturman J.R., Denny W.A. & Wilson W.R. (2003). Multicellular resistance to tirapazamine is due to restricted extravascular transport: a pharmacokinetic/pharmacodynamic study in HT29 multicellular layer cultures. *Cancer Res*, **63,** 5970-7.

15. Phillips R.M., Loadman P.M. & Cronin B.P. (1998). Evaluation of a novel in vitro assay for assessing drug penetration into avascular regions of tumours. *Br J Cancer*, **77,** 2112-9.

16. Cowan D.S. & Tannock I.F. (2001). Factors that influence the penetration of methotrexate through solid tissue. *Int J Cancer*, **91,** 120-5.

17. Tunggal J.K., Melo T., Ballinger J.R. & Tannock I.F. (2000). The influence of expression of P-glycoprotein on the penetration of anticancer drugs through multicellular layers. *Int J Cancer*, **86,** 101-7.

18. Chauhan VP, Lanning RM, Diop-Frimpong B, Mok W, Brown EB, Padera TP, Boucher Y, Jain RK. Multiscale measurements distinguish cellular and interstitial hindrances to diffusion in vivo. Biophys J. 2009 Jul 8;97(1):330-6.

19. Alexandrakis G, Brown EB, Tong RT, McKee TD, Campbell RB, Boucher Y, Jain RK. Two-photon fluorescence correlation microscopy reveals the two-phase nature of transport in tumors. Nat Med. 2004 Feb;10(2):203-7.

20. Jordan M.A. & Wilson L. (2004). Microtubules as a target for anticancer drugs. *Nat Rev Cancer*, **4,** 253-65.

21. Walker J., Martin C. & Callaghan R. (2004). Inhibition of P-glycoprotein function by XR9576 in a solid tumour model can restore anticancer drug efficacy. *Eur J Cancer*, **40,** 594-605.

22. Leighton J.C., Jr. & Goldstein L.J. (1995). P-glycoprotein in adult solid tumors. Expression and prognostic significance. *Hematol Oncol Clin North Am*, **9,** 251-73.

23. Noonan KE, Beck C, Holzmayer TA, Chin JE, Wunder JS, Andrulis IL, Gazdar AF, Willman CL, Griffith B, Von Hoff DD, et al. Quantitative analysis of MDR1 (multidrug resistance) gene expression in human tumors by polymerase chain reaction. Proc Natl Acad Sci U S A. 1990 Sep;87(18):7160-4.

24. Wartenberg M., Ling F.C., Schallenberg M., Baumer A.T., Petrat K., Hescheler J. & Sauer H. (2001). Down-regulation of intrinsic P-glycoprotein expression in multicellular prostate tumor spheroids by reactive oxygen species. *J Biol Chem*, **276,** 17420-8.

25. Wang D and Lippard SJ, Cellular processing of platinum anticancer drugs. *Nat Rev Drug Discov* 4(4): 307-20, 2005.

26. Kartalou M and Essigmann JM, Recognition of cisplatin adducts by cellular proteins. *Mutat Res* 478(1-2): 1-21, 2001.

27. Lindauer E and Holler E, Cellular distribution and cellular reactivity of platinum (II) complexes. *Biochem Pharmacol* 52(1): 7-14, 1996.

28. Dolman RC, Deacon GB and Hambley TW, Studies of the binding of a series of platinum(IV) complexes to plasma proteins. *J Inorg Biochem* 88(3-4): 260-7, 2002.

29. Siddik ZH, Cisplatin: mode of cytotoxic action and molecular basis of resistance. *Oncogene* 22(47): 7265-79, 2003.

30. Holzer AK, Katano K, Klomp LW and Howell SB, Cisplatin rapidly down-regulates its own influx transporter hCTR1 in cultured human ovarian carcinoma cells. *Clin Cancer Res* 10(19): 6744-9, 2004.

31. Katano K, Safaei R, Samimi G, Holzer A, Tomioka M, Goodman M and Howell SB, Confocal microscopic analysis of the interaction between cisplatin and the copper transporter ATP7B in human ovarian carcinoma cells. *Clin Cancer Res* 10(13): 4578-88, 2004.

32. Hall MD, Amjadi S, Zhang M, Beale PJ and Hambley TW, The mechanism of action of platinum(IV) complexes in ovarian cancer cell lines. *J Inorg Biochem* 98(10): 1614-24, 2004.

33. Hicks KO, Ohms SJ, van Zijl PL, Denny WA, Hunter PJ and Wilson WR, An experimental and mathematical model for the extravascular transport of a DNA intercalator in tumours. *Br J Cancer* 76(7): 894-903, 1997.

34. Hall MD, Martin C, Ferguson DJ, Phillips RM, Hambley TW and Callaghan R, Comparative efficacy of novel platinum(IV) compounds with established chemotherapeutic drugs in solid tumour models. *Biochem Pharmacol* 67(1): 17-30, 2004.

35. Kakolyris S., Giatromanolaki A., Koukourakis M., Powis G., Souglakos J., Sivridis E., Georgoulias V., Gatter K.C. & Harris A.L. (2001). Thioredoxin expression is associated with lymph node status and prognosis in early operable non-small cell lung cancer. *Clin Cancer Res*, **7,** 3087-91.

36. Emerson M., Renwick L., Tate S., Rhind S., Milne E., Painter H.A., Boyd A.C., Mclachlan G., Griesenbach U., Cheng S.H., Gill D.R., Hyde S.C., Baker A., Alton E.W., Porteous D.J. & Collie D.D. (2003). Transfection efficiency and toxicity following delivery of naked plasmid DNA and cationic lipid-DNA complexes to ovine lung segments. *Mol Ther*, **8,** 646-53.

37. Rothnie A., Theron D., Soceneantu L., Martin C., Traikia M., Berridge G., Higgins C.F., Devaux P.F. & Callaghan R. (2001). The importance of cholesterol in maintenance of P-glycoprotein activity and its membrane perturbing influence. *Eur Biophys J*, **30,** 430-42.

38. Wilson W.R. & Hicks K.O. (1999). Measurement of extravascular drug diffusion in multicellular layers. *Br J Cancer*, **79,** 1623-6.

39. Kenakin T.P. (1997). *Pharmacologic analysis of drug-receptor interaction*. Philadelphia: Lippincott-Raven.

40. Ilinski P, Lai B, Cai Z, Yun W, Legnini D, Talarico T, Cholewa M, Webster LK, Deacon GB, Rainone S, Phillips DR and Stampfl AP, The direct mapping of the uptake of platinum anticancer agents in individual human ovarian adenocarcinoma cells using a hard X-ray microprobe. *Cancer Res* 63(8): 1776-9, 2003.

41. Brunetti A, del Rio MS, Golosio B, Simionovici A and Somogyi A, A library for X-ray matter interaction cross sections for X-ray fluorescence applications. *Spectrochim. Acta B* 59((10-11)): 1725-1731, 2004.

42. Weinstein R.S., Jakate S.M., Dominguez J.M., Lebovitz M.D., Koukoulis G.K., Kuszak J.R., Klusens L.F., Grogan T.M., Saclarides T.J., Roninson I.B. & *et al.* (1991). Relationship of the expression of the multidrug resistance gene product (P-glycoprotein) in human colon carcinoma to local tumor aggressiveness and lymph node metastasis. *Cancer Res*, **51,** 2720-6.

43. Cussler E.L. (1984). *Diffusion: mass transfer in fluid systems*. Cambridge: Cambridge University Press.

44. Pollack G.L. & Enyeart J.J. (1985). Atomic test of the Stokes-Einstein law. II. Diffusion of Xe through liquid hydrocarbons. *Physical Review. A*, **31,** 980-984.

45. Venturoli D. & Rippe B. (2001). Transport asymmetry in peritoneal dialysis: application of a serial heteroporous peritoneal membrane model. *Am J Physiol Renal Physiol*, **280,** F599-606.

46. Moncrief J.W. & Lipscomb W.N. (1965). Structures of leurocristine (vincristine) and vincaleukoblastine. X-ray analysis of leurocristine methiodide. *J Am Chem Soc*, **87,** 4963-4.

47. Dong J.G., Bornmann W., Nakanishi K. & Berova N. (1995). Structural studies of vinblastine alkaloids by exciton coupled circular dichroism. *Phytochemistry*, **40,** 1821-4.

48. Fleet J.C., Wang L., Vitek O., Craig B.A. & Edenberg H.J. (2003). Gene expression profiling of Caco-2 BBe cells suggests a role for specific signaling pathways during intestinal differentiation. *Physiol Genomics*, **13,** 57-68.

49. Owellen R.J., Hartke C.A. & Hains F.O. (1977). Pharmacokinetics and metabolism of vinblastine in humans. *Cancer Res*, **37,** 2597-602.

50. Trédan O, Garbens AB, Lalani AS, Tannock IF. The hypoxia-activated ProDrug AQ4N penetrates deeply in tumor tissues and complements the limited distribution of mitoxantrone. Cancer Res. 2009 Feb 1;69(3):940-7. Epub 2009 Jan 27.

51. Hicks K, Siim BG, Jaiswal JK, Pruijn FB, Fraser AM, Patel R, Hogg A, Liyanage HD, Dorie MJ, Brown JM, Denny WA, Hay MP, Wilson WR. Pharmacokinetic/pharmacodynamic modeling identifies SN30000 and SN29751 as tirapazamine analogs with improved tissue penetration and hypoxic cell killing in tumors. Clin Cancer Res. 2010 Aug 20.

52. Cotran R.S., Kumar V., Collins T. & Robbins S.L. (1999). *Robbins pathologic basis of disease*. Philadelphia; London: Saunders.

53. Saraste A. (1999). Morphologic criteria and detection of apoptosis. Herz, 24, 189-95.

54. Cowan DS, Hicks KO, Wilson WR. Multicellular membranes as an in vitro model for extravascular diffusion in tumours. Br J Cancer Suppl. 1996 Jul;27:S28-31.

55. Hicks KO, Pruijn FB, Secomb TW, Hay MP, Hsu R, Brown JM, Denny WA, Dewhirst MW, Wilson WR. Use of three-dimensional tissue cultures to model extravascular transport and predict in vivo activity of hypoxia-targeted anticancer drugs. J Natl Cancer Inst. 2006 Aug 16;98(16):1118-28.

56. Swabb E.A., Wei J. & Gullino P.M. (1974). Diffusion and convection in normal and neoplastic tissues. Cancer Res, 34, 2814-22.

57. Davies Cde L., Berk D.A., Pluen A. & Jain R.K. (2002). Comparison of IgG diffusion and extracellular matrix composition in rhabdomyosarcomas grown in mice versus in vitro as spheroids reveals the role of host stromal cells. *Br J Cancer*, **86,** 1639-44.

58. Prokopova-Kubinova S., Vargova L., Tao L., Ulbrich K., Surb V., Sykova E. & Nicholson C. (2001). Poly[N-(2-hydroxypropyl)methacrylamide] polymers diffuse in brain extracellular space with same tortuosity as small molecules. *Biophys J*, **80,** 542-8.

59. Tao L. & Nicholson C. (2004). Maximum geometrical hindrance to diffusion in brain extracellular space surrounding uniformly spaced convex cells. *J Theor Biol*, **229,** 59-68.

60. Erlichman C. & Wu A. (1992). Resistance of MGH-U1 bladder cancer spheroids to vincristine. *Anticancer Res*, **12,** 1233-6.

61. Hall MD, Dillon CT, Zhang M, Beale P, Cai Z, Lai B, Stampfl AP and Hambley TW, The cellular distribution and oxidation state of platinum(II) and platinum(IV) antitumour complexes in cancer cells. J Biol Inorg Chem 8(7): 726-32, 2003.

62. Lottner C, Knuechel R, Bernhardt G and Brunner H, Distribution and subcellular localization of a water-soluble hematoporphyrin-platinum(II) complex in human bladder cancer cells. Cancer Lett 215(2): 167-77, 2004.

63. Nishikawa K, Newman RA, Murray L, Khokhar AR and Rosenblum MG, Detection of cellular platinum using the monoclonal antibody 1C1. Mol Biother 2(4): 235-41, 1990.
64. Noble CO, Krauze MT, Drummond DC, Yamashita Y, Saito R, Berger MS, Kirpotin DB, Bankiewicz KS and Park JW, Novel nanoliposomal CPT-11 infused by convection-enhanced delivery in intracranial tumors: pharmacology and efficacy. *Cancer Res* 66(5): 2801-6, 2006.
65. Newton HB, Intra-arterial chemotherapy of primary brain tumors. *Curr Treat Options Oncol* 6(6): 519-30, 2005.
66. Crank J. (1975). *The mathematics of diffusion*. Oxford: Clarendon Press.
67. Kalayda GV, Jansen BA, Molenaar C, Wielaard P, Tanke HJ, Reedijk J. Dinuclear platinum complexes with N, N'-bis(aminoalkyl)-1,4-diaminoanthraquinones as linking ligands. Part II. Cellular processing in A2780 cisplatin-resistant human ovarian carcinoma cells: new insights into the mechanism of resistance. J Biol Inorg Chem. 2004 Jun;9(4):414-22.

9. Acknowledgement

I am greatly thankful to my supervisors. Prof. Zita Borbényi initiated the collaboration between the Departments and together with Prof. Andrea Rita Horváth supported my initial application for the Eötvös Fellowship submitted to the “Magyar Ösztöndíj Bizottság”. I am indebted to Dr. Richard Callaghan for allowing me to work in his lab, for his expert guidance, ongoing support and wise leadership. I am also thankful to the CRUK for financing most of my work through grants held by RC. Furthermore, I thank Tiina Roose and her Master’s student Phil Hyde from the Math’s Department at The University of Oxford. I would like to express my gratitude to the past and present leaders of my clinical department, namely Prof. Miklós Csanády, Prof. Tamás Forster and the past leader of the haematology team Prof. Gyula Varga. I am grateful to my colleagues in Oxford, amongst many others Cathrine Martin, Andy Taylor, Howard Mellor, Ian Kerr, Janet Storm, Alice Rothnie, Mark Gabriel and Rachel Scott for her excellent work on the platinum compounds. I wish to acknowledge our collaborators Bob Ford, Matt Hall, Margaret Jones, Roger Phillips, Heidi de Wet and Lee Davies. I am also greatly indebted to my colleagues in Szeged, who supported this project: Klára Piukovics, Imelda Marton, Nóra Adamkovich, Tímea Gurbity Pálfi, Mihály Gurzó, Anita Szőke. Last but not least I would like to thank my family for all the support and patience over the last decade.